Ion–Cement Hydrates Interactions Governed Multi–Ionic Transport Model for Cementitious Materials

Y. Elakneswaran*, A. Iwasa, T. Nawa, T. Sato, K. Kurumisawa,

Division of Sustainable Resources Engineering,

Faculty of Engineering, Hokkaido University,

Kita–Ku, Kita 13, Nishi 8, Sapporo, Hokkaido,

Japan, 060–8628

* Corresponding author:

E–mail: laknesh@eng.hokudai.ac.jp

TEL: +81–11–706–6326, Fax: +81–11–706–7274

Abstract

The main objective of this investigation is to describe the interaction between cement hydrates and electrolyte solution to understand multi–ionic transport in cementitious materials. A surface complexation model in PHREEQC including an electrostatic term is used to simulate the ionic adsorption on the calcium silicate hydrate (C–S–H) surface. The equilibrium constants for the adsorption of ions on C–S–H surfaces are obtained by fitting experimental data to the model. The adsorption of both divalent and mono–valent cations, and also anions significantly changes the surface charges of hydrated paste. Chloride is being held in a chemical binding as Friedel's salt and bound mainly by the adsorptive action of C–S–H. An integrated modelling approach employing a phase–equilibrium model, a surface complexation model, and a multi–component diffusion model has been developed in PHREEQC to simulate the multi–ionic transport through hydrated cement paste. It was found that the physical adsorption of ions on C–S–H, the size of pores, and the surface site density of C–S–H govern the rate of penetration of ionic species. Finally, the proposed model has been validated against chloride profiles measured in this study as well as with data available in the literature for hydrated cement paste.

Keywords: Adsorption; Diffusion; Durability; Modelling; PHREEQC

1. Introduction

Chloride induced corrosion has been recognized as the most critical problem in the deterioration of reinforced concrete structures exposed to chloride–rich environments through application of de–icing

salts or from the natural environment and it has still not been fully understood despite much research [1–3]. Chloride ingress through covercrete to the reinforcement depends on the material properties as well as on environmental factors [1]. Chloride ions can penetrate into concrete from the environment surrounding a structure by several mechanisms: diffusion, capillary suction, advection, migration, and others. Diffusion is the predominant transport mechanism by which chlorides are transported through pores in saturated cementitious materials in the absence of an electric field. Chloride penetrates into the concrete accompanied by other ions, and other ionic species directly influence the chloride transport. To elucidate the mechanisms involved, it is therefore necessary to consider the ion–ion interaction in the ionic transport.

There are a number of models for simulation of the ionic transport into cementitious materials [4–9]. These models are improving the understanding of ionic transport phenomena by considering different aspects of the mechanisms and the coupling between them. Over the years, Nernst–Planck/Poisson equations have been successfully applied to evaluate the electrical coupling between ions in dilute solution as well as in concentrated solutions where the chemical activity effects are significant [4–8]. Samson *et al.* further modified the ionic transport model for an unsaturated cement system [5]. Johannesson *et al.* proposed a model for multi–species diffusion considering chemical reactions between cement hydrates and pore solution through ion exchange reactions [6]. In addition, Hosokawa *et al*. have developed a multi–species model that includes the binding of ions on cement hydrates and precipitation/dissolution of cement hydrates [7]. However, in these investigations, ionic concentration changes within the pores were not taken into account. The concentrations of ions near the surface are significantly influenced by the surface electrical charge or surface potential. Evaluating the existing models of the prediction of multi–ionic transport into cementitious materials, makes it clear that further research is needed on this topic. The existing models are limited in terms of surface complexation reactions and the effects of surface properties of cement hydrates on multi–ionic transport. The

presence of an electric charge at the solid/solution interface has a significant influence on ionic diffusion; however, this well–known feature has not been accounted for in the current models. The transporting ionic species can interact with cement hydrates, either physically to the cement gel or chemically. Therefore, the presence electric charge at the solid/solution interface is another important factor that must be considered in ionic transport.

The mechanisms of surface charge behaviour in cement hydrates and the properties of interfaces between solid surfaces and pore solution have been discussed in very few studies. Cementitious materials, like other minerals, develop an electrical charge on the surface when it is in contact with electrolyte solutions. It can be considered that the formation of a surface electrical charge is due to a combination of ionization, dissolution, and ionic adsorption. The surface charge is closely related to the surface potential; however, there has been no way to measure surface potential directly. The net surface charge and sign can be determined by measuring the membrane potential between surfaces [10]. Zhang and Buenfeld measured the membrane potential across hydrated cementitious materials and its influence on chloride transport [11–12]. The conclusions were that the measured membrane potential is affected by binder type and kind of exposure solution. Further, a positive membrane potential accelerates chloride diffusion and a negative membrane potential decelerates chloride diffusion. However, there is a lack of results on the sign and magnitude of the surface charge of cementitious materials. The hydrated cement paste has a positive surface charge with or without the presence of blast furnace slag [13–14]. An Electrical Double Layer (EDL) forms at the solid/solution interface because of the surface charge. The zeta potential (ζ) is defined as the potential at a shear plane located between adsorbed and diffuse layers in EDL. Much research has been carried out to determine ζ in cementitious materials mainly in cements and synthetic C–S–H suspensions as well as in mineral admixtures [15–20]. The EDL on C–S–H surface plays an important role in several applications in cementitious materials. The interaction between the ingress of ionic species and cement hydrates is influenced by the

physical and chemical properties of the pore systems. Some research has highlighted the influence of EDL properties on ionic diffusion [9, 16, 21–24]. Chatterji and Kawamura estimated the thickness of EDL and its characteristics on ionic transport [16]. Two ionic diffusion processes occur in the cement paste: one through EDL and the other through the bulk solution. They reported that anions diffuse through the bulk solution and cations through the EDL where the concentrations of cations are high. Friedmann proposed a physical model for EDL effects on multispecies transport in cementitious materials [24]. Here, gel pores influence the transport of ions strongly due to overlapping double layers. Further, mean concentrations of cations and anions can be different across cross sections of pores with overlapping EDL. In salt solution, diffusing chloride ions are much more affected by the surface charge than sodium ions in mature cement paste [9, 22]. It is generally known that the porosity of cementitious materials significantly influences chloride transport. However, the total pore volume does not make any relationship with the measured apparent diffusion coefficient of chloride in mature cement paste [9, 14]. Goto *et al.* proposed a model for the EDL in hydrated cement paste [9]. This model can explain why the apparent diffusion coefficients of cations are lower than that of anions in hydrated cement paste. However, the model fails to explain the mechanisms quantitatively in terms of ionic transport. Our previous work has reported some quantitative relationships between the net positive surface charge of hydrated cement paste and the apparent diffusion coefficient of chloride [13–14]. To have a better understanding of multi–ionic transport into cementitious materials, it is necessary to establish the importance of the effect of EDL properties on ionic ingress to be able to evaluate the durability performance of concrete. Thus, the primary objective of the research here is to investigate the interaction between cement hydrates and electrolyte solution to elucidate the multi–ionic transport mechanisms in cementitious materials. This is achieved through a modelling approach as well as through detailed experimental programs.

2. Materials and methods

2.1 Materials and sample preparation

All experiments were performed using Ordinary Portland Cement (OPC). Hydrated cement paste (HCP) samples with a water to cement ratio of 0.5 were cast in cylindrical moulds with a diameter of 50 mm and a length of 100 mm. The samples were cured in saturated calcium hydroxide solution for 91 days. After the curing, different kinds of sample preparation were carried out for different experiments. For Electron Probe Micro Analysis (EPMA) experiments, a thickness of around 5 mm of one sample was cut and removed, and the remaining part of the sample was used. The cut surface was exposed to chloride solution, and the other surfaces were coated with epoxy resin to ensure only one direction of chloride penetration. Then the EPMA sample was exposed to artificial seawater for 91 days at 20 °C. The composition of the seawater is given in Table 1. After the seawater exposure, the sample was cut into two halves parallel to the direction of the ionic ingress. Further, a 40 mm long 30 mm wide and 5 mm thick portion was cut from the surface exposed to chloride and used for EPMA mapping. The slice was set in epoxy resin and polished smooth. Isopropanol was used during the cutting and polishing to minimize any effect on the chloride distribution. The polished sample was vacuum dried for three days, and carbon coating was applied before the EPMA mapping. The other half piece was used to determine the amount of chloride by a traditional method. It was sliced perpendicular to the direction of chloride penetration at 10 mm intervals, and the size of the three slices were 30 mm * 10 mm * 10 mm. The slices were ground by ball mill, and around 5 g of each sample was used to determine the chloride content. Sample preparation and other experimental techniques are described in more detail elsewhere [25]. Briefly, ζ measurements were carried out for less than 45 μm HCP powder. Suspensions were prepared at 0.1 g/l solid to liquid, and a Zetasizer Nano series apparatus was used to determine ζ

through the Smoluchowski approximation. The porosity and pore size distribution were determined through Mercury Intrusion Porosimetry (MIP) (for pore diameters > 6 nm) and nitrogen gas adsorption (for pore diameters < 6 nm) techniques. Cylindrical samples were prepared to extract pore solution; the extraction was performed using a steel die method. Shortly after the extraction, the chemical composition was analysed using ion chromatography and ICP.

2.2 EPMA measurements

An EPMA JEOL JXA–8900M apparatus was used to carry out element mapping in HCP. The measurement conditions were 15 kV accelerating voltage, 50 nA beam current, pixel size 60 μm * 30 μm, and 1000 * 50 points. The chloride profile was calculated from the mapping, but it was expressed as X–ray counts of chloride. The counts were corrected by the determining chloride concentration from a wet analysis as described in Japanese Industrial Standard (JIS) A 1154. In the wet analysis, powder samples were mixed with 2 mol/l nitric acid solution and boiled for five minutes. The boiled solution was filtered and the concentration of chloride in the solution was measured with ion chromatography.

2.3 Modelling approach

The geochemical transport code PHREEQC is used to simulate multi–ionic transport in HCP. In this study, an integrated thermodynamic model is proposed to consider ion–ion interactions as well as ion–solid interactions in the multi–ionic transport. Further, the model is implemented in PHREEQC using the phase–equilibrium, surface complexation, and multi component diffusion (MCD) modules. The thermodynamic properties of various minerals and aqueous species are used as reported in the BRGM

database (Thermoddem) [26].

2.3.1 Phase–equilibrium model

This model is used to define the amount of cement hydrate phases that can react reversibly with an aqueous solution to achieve equilibrium. The phases will dissolve or precipitate to achieve the equilibrium or will dissolve completely. The equilibrium reactions are expressed by the mass–action equations in PHREEQC using the extended Debye–Huckel activity model [27]. Cement hydrate phases are defined by chemical reactions, an equilibrium constant, and enthalpy. The thermodynamic equilibrium constant, K_T, at a given temperature T can be expressed as:

$$K_T = \exp\left(-\frac{\Delta_r G_T^0}{RT}\right) \quad (1)$$

Where R is the universal gas constant equal to 8.31451 J/(mol.K) and $\Delta_r G_T^0$ is the standard Gibbs energy of reaction at temperature T:

$$\Delta_r G_T^0 = \sum \Delta_f G_{T,products}^0 - \sum \Delta_f G_{T,reactants}^0 \quad (2)$$

Here $\Delta_f G_T^0$ is the Gibbs free energy of formation for a species at a given temperature T. Explanations on basic principles of the thermodynamic calculations and chemical reactions are as given in textbooks [27–28]. The thermodynamic properties of cement hydrates are prepared in PHREEQC format using the standard thermodynamic properties of aqueous solutions and standard molar thermodynamic

properties of cement hydrates given in ref. [29]. The calculated values of the equilibrium constant (log_K_T) and the standard heat of reaction ($\Delta_r H^o$) for the dissolution reaction of cement hydrates are given in Table 2. The input data include the name of the phase (defined by chemical reaction, equilibrium constant (log_K_T), and standard heat of reaction ($\Delta_r H^o$), as given in Table 2), the specified saturation index (with a value of zero at the equilibrium), and the amount of the phase present in moles. In this study, the phase–equilibrium model is applied for thermodynamic equilibrium reactions between cement hydrates and initial pore water as well as the equilibrium reactions between cement hydrates and exposure solution.

2.3.2 Surface complexation model for ionic adsorption

The PHREEQC, which considers the surface complexation reactions through mass–action equations, mole–balance equations for surface sites, and charge–potential relations for surfaces, is used to determine the ionic adsorption on C–S–H [30]. A generalized two–layer model in PHREEQC has been incorporated for surface complexation reactions [31]. In the model, all specifically adsorbed ions are assigned to a surface layer and non–specifically adsorbed ions are assigned to a diffuse layer. The Gouy–Chapman theory is assumed to hold for the ionic distribution in the diffuse layer. Further, the model assumes that the activity of the surface species is numerically equal to their concentration. The surface charge is caused by ionization of all surface sites through proton exchange reactions as well as surface coordination reactions with cations and anions. The surface charge density is the amount of charge per area of the surface [31]:

$$\sigma = \frac{F}{AS}[(\equiv XOH_2^+) + (\equiv XOM^+) - (\equiv XO^-) - (\equiv XA^-)] = F[\Gamma_H - \Gamma_{OH} + \sum(Z_M\Gamma_M) + \sum(Z_A\Gamma_A)] \quad (3)$$

Where F is the Faraday constant (96,485 C/mol), A is the specific surface area (m^2/g), S is the solid concentration (g/l), Z is the valence of an adsorbing ion, Γ_H and Γ_{OH} are the adsorption densities of protons and hydroxyl ions (mol/m^2), and Γ_M and Γ_A are the adsorption densities of specifically adsorbed cations and anions. According to Gouy–Chapman theory (for a symmetrical electrolyte with valence Z), the surface charge density (σ (C/m^2)) is related to the surface potential (ψ_0 (V)) by:

$$\sigma = \left(8000\varepsilon\varepsilon_0 RTc\right)^{\frac{1}{2}} \sinh\left(\frac{ZF\psi_0}{2RT}\right) \tag{4}$$

Where R is the universal gas constant, T is the absolute temperature (K), ε is the dielectric constant of water (dimensionless), ε_0 is the permittivity of free space ($8.854 * 10^{-12}$ C/V.m), and c is the molar electrolyte concentration.

This model can calculate the surface potential and the amount of adsorbed ions when a C–S–H surface is in contact with an ionic solution. Thus, the surface site density of C–S–H is an important parameter in the model because it is directly related to the surface charge density. The surface properties of cement hydrates are much less known than those of other OH bearing oxides like silicates or alumina. The crystal structure of the C–S–H phase has not been fully determined, but may be close to the Tobermorite or Jennite structure [32]. Considering the structure of C–S–H, Pointeau *et al.* have reported that C–S–H has two kinds of surface sites called silanol (≡ SiOH) and silandiol (= $Si(OH)_2$ sites [20]. Silanol sites are present on silicate tetrahedra at the end of the silicate chain, and silandiol sites are present in the middle of the chain on bridging tetrahedra. Viallis－Terrisse *et al.* model considered that the whole surface of C–S–H consists of sites of one type (≡ SiOH) [19]. Further, the thermodynamic model in Heath *et al.* assumed that the surface of C–S–H is dominated by two sites:

silanol (≡ SiOH) and calcium (– CaOH) sites [33]. It can be concluded that the types and amounts of surface sites on C–S–H have not been fully clarified. More elaborate models and experimental techniques are needed to understand the details of the surface sites of C–S–H more fully. In the following, this study assumes that the surface of C–S–H consists only one type of site which is here called the silanol site (≡ SiOH), and the density of the silanol site can be calculated according to the silicate structural model of C–S–H presented by Viallis－Terrisse. *et al.* [19].

2.3.3 Multi component diffusion model

The diffusion coefficients of cations, anions, and neutral species in pore water of cementitious materials have different values. The existence of the EDL on the surface of cement hydrates plays an important role in the magnitudes of these dissimilar values. In cementitious materials, anions and cations have different paths of diffusion: anions diffuse through free solution while diffusion of cations takes place through a diffuse double layer (DDL). The MCD module available in PHREEQC can be used to simulate the ionic transport in cementitious materials because it accurately simulates the multicomponent diffusion through free solution as well as through DDL. The basic theory for calculating MCD for all species is described elsewhere [34]; the main governing equations are presented briefly here. The electrochemical potential of a species *i* is given by:

$$\mu_i = \mu_i^0 + RT \ln(a_i) + z_i F \psi \tag{5}$$

Where μ_i^0 is the standard electrochemical potential (J/mol), a_i is the activity, R is the universal gas constant, T is the absolute temperature, z_i is the charge number, F is the Faraday constant, and ψ is the

electrical potential (V). The diffusive flux of an ion *i* in a solution due to chemical and electrical potential gradients can be expressed as:

$$J_i = -\frac{u_i c_i}{|z_i| F}\frac{\partial \mu_i}{\partial x} - \frac{u_i z_i c_i}{|z_i|}\frac{\partial \psi}{\partial x} \tag{6}$$

Where J_i is the flux of a species *i* (mol/m^2/s), c_i is the concentration of ion *i*, and u_i is the mobility of ion *i* in water (m^2/s/V). The mobility is related to the tracer diffusion coefficient $D_{w,i}$ (m^2/s) by:

$$D_{w,i} = \frac{u_i RT}{|z_i| F} \tag{7}$$

If there is no electrical current, $\sum z_i J_i = 0$. The zero charge flux condition permits the expression of the electrical potential gradient as a function of the other terms in Eq. (6) and the diffusive flux, J_i, is given as:

$$J_i = -D_{w,i}\left[\frac{\partial \ln(\gamma_i)}{\partial \ln(c_i)} + 1\right]\frac{\partial c_i}{\partial x} + D_{w,i} z_i c_i \frac{\sum_{j=1}^{n} D_{w,j} z_j \left[\frac{\partial \ln(\gamma_j)}{\partial \ln(c_j)} + 1\right]\frac{\partial c_j}{\partial x}}{\sum_{j=1}^{n} D_{w,j} z_j^2 c_j} \tag{8}$$

Where the subscript *j* is introduced to show that these species are for the potential term.

The DDL can be explicitly considered in the PHREEQC MCD calculations. All pores are considered to have one size, and it is subdivided through length as a paired cells. Each pair contains a charge–balanced free solution layer and a DDL together with the charged surface. The solutes in the cells are

assumed to be in equilibrium according to Boltzmann's formula with zero potential in the charged free solution and a potential that is optimized to give zero charge in the DDL. Paired cells are aligned along the pore, and multicomponent diffusion is calculated by explicit finite differences for each interface among the pairs of cells [34]. The concentrations of ions in the DDL are related to the ionic concentration in the free solution through Boltzmann's equation considering the Donnan approximation:

$$c_{DDL,i} = c_i \exp\left(\frac{-z_i F \psi_{DDL}}{RT}\right) \tag{9}$$

Where $c_{DDL,i}$ is the concentration of ion i in DDL. The electroneutrality condition is achieved in the DDL through:

$$\sum z_i c_{DDL,i} + \sigma_{DDL} = 0 \tag{10}$$

The above Eq. (8) can be used in the free solution as well as in the DDL; only the concentrations of ions differ in the free solution and the DDL. The MCD can be incorporated in PHREEQC with the keyword "–multi_d".

In the proposed model, the MCD model is applied with two other models which take into account the phase–equilibrium and surface complexation reactions. It is assumed that the HCP can be considered as an assemblage of four main hydrates: C–S–H, portlandite, ettringite, and monosulfoaluminate. The mass percent of the amorphous component is equal to the C–S–H mass percent. The simulation commences with the phase–equilibrium reactions: the pore solution of HCP is equilibrated with the cement hydrates. As a result of dissolution or precipitation of the cement hydrates, the concentration

and pH of the pore solution changes, and the modified pore solution is used in the initial surface reaction calculations. The surface reactions of C–S–H with the major ions are considered in the surface complexation model. The exposure solution is in equilibrium with the cement hydrates before it enters into the pore solution. Thus, the concentration of the exposed solution changes with the thermal equilibrium. This solution then enters into the HCP where C–S–H surface sites are present, and there are surface complexation reactions between the transporting ions and surface sites. The MCD module calculates fluxes for all species separately in the charged free solution and in the DDL, and then sums them up for the interface between two cells. In the case of HCP, the length of a single pore is subdivided into a number of immobile cells, and one–dimensional ionic transport takes place from the solution of exposure to the pore solution.

3. Results and discussions

3.1 Prediction of equilibrium constants for ionic adsorption on C–S–H

The main hydration product of cementitious materials, C–S–H, is made up of silicates and consists of silanol (≡ SiOH) surface groups. The surface groups contain all the reactive sites available for release or adsorption of protons and also for adsorption of cations and anions. A solution in equilibrium with C–S–H has a very high pH due to calcium leaching, and the surface of C–S–H particles reacts with hydroxide ions to form negative charges according to the dissociation reaction:

$$\equiv SiOH + OH^- \Leftrightarrow \equiv SiO^- + H_2O \qquad K_1 = \frac{a_{SiO^-}}{a_{SiOH} * a_{OH^-}} \exp(-\frac{F\psi_0}{RT}) \qquad (11)$$

Several studies have suggested that calcium ions behave as the potential determining ions on the C–S–H surface and lead to a charge reversal [17–20]. In this case, the surface charges of the C–S–H particles are neutralized by the calcium ions which lose some of their hydrated water molecules and form ionic bonds with silanol sites through the inner–sphere complexation reaction:

$$\equiv SiOH + Ca^{2+} \Leftrightarrow \equiv SiOCa^{+} + H^{+} \qquad K_2 = \frac{a_{SiOCa^{+}} * a_{H^{+}}}{a_{SiOH} * a_{Ca^{2+}}} \exp(\frac{F\psi_0}{RT}) \qquad (12)$$

The generalized two–layer surface complexation model in PHREEQC can be used to simulate this calcium adsorption on the C–S–H surface, and the simulated results with electrophoretic experimental data for HCP in calcium hydroxide solutions are shown in Fig. 1. The HCP particles move as they are negatively charged at relatively low pH values (10.5－11.0) or at low concentrations of calcium, but at higher pH values (above 11.1) or at high calcium concentrations they move as positively charged particles. The Iso Electric Point (IEP), where the charge reversal occurs, is located at a pH of around 11.1. At pH values above this, further adsorption of calcium would result in a strong positive charge density of the C–S–H. The simulated results on the calcium adsorption are fitted to the measured values of ζ, and the equilibrium constants for Eqs. (11) and (12) are －12.7 and －9.4 respectively. Further details on the calculation of equilibrium constants for calcium adsorption on the C–S–H have been presented in a previous paper [25].

Chloride interacts with cement hydrates chemically as well as physically: the conversion of hydroxyl AFm to Friedel's salt by ion exchange is considered to be chemical binding [35], while the adsorption of chloride on the surface of cement hydrates by van der Walls and electrostatic forces is considered to be physical binding. The physical adsorption of chlorides on HCP is dominant in C–S–H. In chloride solutions, a part of the silanol surface groups are dissociated according to Eq. (11), enabling chloride

ions to adsorb on the unionized silanol groups via the inner–sphere complexation reaction:

$$\equiv SiOH + \quad Cl^{-} \Leftrightarrow \equiv SiOHCl^{-} \tag{13}$$

The measured ζ values of HCP suspensions in different chloride solutions are presented in Fig. 2. The ζ of the HCP suspensions are negative and the absolute values increase with the concentration of the chloride. The negative values of ζ are due to dissociation of cement hydrates as well as the adsorption of chloride on C–S–H. The dissociation of C–S–H does not give a large change with chloride concentration, because of the constant pH. Therefore, the physical adsorption of chloride on C–S–H is responsible for an increase in the absolute values of ζ with increases in the chloride concentrations. Further, at higher concentrations of chloride in the solution, the chloride itself begins to contribute to the ionic strength of the solution and the absolute values of ζ diminish. The chloride adsorption on C–S–H is analyzed with the surface complexation model, and the calculated equilibrium constant for Eq. (13) is -0.35. Further, chloride can adsorb on silanol sites where calcium is adsorbed ($SiOCa^{+}$) through the reaction:

$$\equiv SiOH + Ca^{2+} + Cl^{-} \Leftrightarrow \equiv SiOCaCl + H^{+} \tag{14}$$

Details of the surface complexation model on chloride adsorption were presented in the previous paper devoted to predicting physical adsorption of chloride on the C–S–H surface [25].

The difference in the ζ values among sodium, potassium, and cesium solutions for the same concentration of chloride in Fig. 2 are due to the adsorption of chloride together with the associated cations. The better adsorbability of the cesium can be explained by the free energy of hydrated cesium

ions being much lower than that of sodium ions [18]. As a result, cesium ions are more easily dehydrate (fully or partially) in an electric field and this affects the ζ of the CsCl suspensions, while sodium ions remain hydrated. In this study, the sodium and potassium adsorption on C–S–H are modelled using the experimental data in [36]. It is assumed that sodium or potassium adsorbs on the surface of C–S–H via inner–sphere complexation reactions. Stoichiometric reactions for the adsorption of sodium and potassium occur according to:

$$\equiv SiOH + Na^{+} \Leftrightarrow \equiv SiONa + H^{+} \quad (15)$$

$$\equiv SiOH + K^{+} \Leftrightarrow \equiv SiOK + H^{+} \quad (16)$$

The mechanism of the cationic adsorption may be assumed to neutralize the negative surface charge of C–S–H. Fig. 3 shows the sodium adsorption isotherm on C–S–H for a calcium to silicon molar ratio (C/S) of 1.5. The equilibrium constants for adsorption of sodium and potassium are derived by fitting the experimental adsorption data in [36] to the simulated results. The equilibrium constants for the adsorption of both sodium and potassium give similar values and those values arrange in a linear relationship with the C/S ratio of C–S–H, as shown in Fig. 4. At low C/S ratios of C–S–H, there is more adsorption of sodium or potassium on the surface of C–S–H, but the adsorption capacity of sodium or potassium is lower at higher C/S ratios of C–S–H.

3.2 Modelling results for multi–ionic transport through electrically charged hydrated cement paste

The ionic concentrations near a charged surface relate to an electrostatic potential through the familiar

Boltzmann equation (Eq. (9)). When the surface potential is known, this equation can be used to determine the distributions of co–ions and counter ions near the charged surface. Fig. 5 shows the ionic distribution close to a negatively charged surface when it is immersed in 0.1 M NaCl. Counter ions are attracted towards the charged surface while co–ions are repelled by the surface, and a diffuse layer forms at the solid/solution interface. Further, the concentrations of both co–ions and counter ions reach the bulk concentrations at a distance equal to five times the Debye length. Based on the results in Fig. 5, it can be inferred that there is no diffuse layer in the vicinity of a charged surface at a distance five times the Debye length as also supported by Chatterji and Kawamura [16]. The surface of hydrated cement paste, with a pore diameter of less than around 7 nm, would be completely covered with the diffuse layer because the Debye length calculated from the ionic strength of the pore solution is nearly 0.7 nm (Table 3). Some recent studies show that the chloride ion is symmetrically solvated in clusters containing up to 255 water molecules, and the cluster size would be around 2–3 nm [37–38]. Therefore, the surface electrical properties would influence the transport of chloride through a pore opening, which is less than around 10 nm. In this study, it is assumed that the size of the gel pores is less than 10 nm in diameter. The pore size distribution from the MIP and nitrogen gas adsorption techniques show that more than 30% of the total pore volume of hydrated cement paste is at pore diameters below 10 nm (Table 4). Thus, hydrated cementitious paste has a considerable amount of gel pores, and the interaction between the electrokinetic properties and ingress of chloride ions cannot be negligible in the pores.

In the simulation, a cylindrical 50 mm diameter and 100 mm high HCP sample was immersed in one litre of artificial seawater for one year. The proposed model includes diffusion of Cl^{-}, Na^{+}, Ca^{2+}, K^{+}, SO_4^{2-}, Mg^{2+}, and OH^{-}species and their interactions with cement hydrates (C–S–H, portlandite, ettringite, and monosulfoaluminate). The physical adsorption of Ca^{2+}, Cl^{-}, Na^{+}, and K^{+} on C–S–H are considered through the reactions given in Eqs. (11)–(16). Each of the ionic species has a self–diffusion coefficient in free water for a specified temperature [39]. The self–diffusion coefficient of ions in free

water and the compositions of the artificial seawater are given in Table 1. The ions in equilibrated seawater (the seawater after attaining equilibrium with the cement hydrates) enter into the pore solution of the HCP. The ionic concentrations in the pore solution are given in Table 3. Initial and final boundary conditions are set to the equilibrated seawater concentrations and zero flux respectively. The shape of the pores is assumed to be cylindrical, and the pore size distributions of the HCP are tabulated in Table 4. As stated in the previous paragraph, the surface electrical charge significantly influences the diffusion of ions through the gel pores, and therefore the simulations are carried out only for the gel pores (< 10 nm). The simulated concentration profiles of the multi–species transport through the gel pores of the HCP are shown in Fig. 6. It can be seen that the ionic concentration profiles depend on both ion–ion and ion–solid interactions. Only ion–ion interactions occur in the ionic transport through the free solution; however, both ion–ion and ion–solid interactions take place in the DDL. It is important to bear in mind that the transport of each ionic species is significantly influenced by the presence of other ionic species as well as by the interaction between the cement hydrates and the ionic species. The proposed intergraded model also includes the Donnan effect at the interface between HCP and the exposed solution. At reaching the Donnan equilibrium, the concentration of the solution near the HCP surface is changed: in this part of the solution, the concentration of counter ions and co–ions are respectively stronger and weaker than in the bulk exposure solution. This can clearly be seen in Fig. 6 at the exposed surface (at the zero distance). The proposed model also predicts changes in the cement hydrates inside the sample during the ionic transport, shown Fig.7. Portlandite and monosulfoaluminate dissolve near the exposed surface, however, Friedel's salt forms. Further, there is no decalcification of C–S–H due to ionic transport.

3.3 Effect of the various parameters on ionic ingress

3.3.1 Influence of physical adsorption

The physical adsorption of the ions has a significant impact on ionic transport. The surface charge of C–S–H plays an important role in the physical adsorption of ions and leads to changes in the ionic concentration profiles in the pore solution. The physical adsorption of ions on the C–S–H is implemented in the proposed model through the surface complexation reactions (Eqs. (12)–(16)). To evaluate the influence of physical adsorption on the ionic transport, the simulation other than physical adsorption of ions is considered in the model. The simulated concentration profiles of anions and cations in the pore solution are shown in Figs. 8 and 9 respectively. It can clearly be seen that ionic adsorption decreases the concentration of both anions and cations in the pore solution. Ionic species are transported through the pore solution by an electrochemical gradient but the adsorption reduces the concentration of these species in the solution. Figs. 8 and 9 indicate that the chloride adsorption influences the concentration of chlorides as well as of other ions (shown by the broken line). In other words, the physical adsorption of chloride reduces the concentrations of not only chloride but also the other ions in the pore solution.

3.3.2 Influence of pore size

The existence of the EDL in the gel pores influences ionic transport more than in the capillary pores. For cement paste with low porosity, the capillary pores are connected with the gel pores [40], and to move through the capillary pores, ions must pass through the gel pores and are subjected to EDL effects in their transport. Further, the occurrence of EDL overlapping is another factor to consider in the ionic

transport through the gel pores. To evaluate the influence of pore size on ionic transport, two ranges of pores (< 10 nm and 10–16.7 nm) with the same porosity are considered. The simulated total content of chloride in these two size ranges of pores is shown in Fig. 10. It can be seen in the figure that there is a high content of chloride near the surface for the gel pores (< 10 nm), higher than that of the other range of pores. In the gel pores, the interaction between chloride and surface charge is much more significant than in the capillary pores. This can be explained by the physical adsorption of chloride on the surface of the C–S–H because the gel pores have a high specific surface area resulting in a large amount of adsorption of chlorides. In the capillary pores, the physical adsorption of chloride is very low but there is a considerable amount of free chlorides. Thus, an important point is to underline that the gel pores can play a significant role in the ionic transport through cementitious materials.

3.3.3 Influence of surface site density

The surface site density C–S–H is an important parameter for the surface complexation reactions in the proposed model. Surface charge or surface site density exerts a strong effect on the physical adsorption of ions as well as on the formation of the EDL. Fig.11 shows the simulated total content of chloride for arbitrary values of silanol site densities. The figure shows that the total content of chloride is dependent on the silanol site density. Further, a higher silanol site density causes an increase in total chloride content near the exposed surface but the trend is opposite a few millimetres away from the surface. The higher silanol site density forms a higher surface charge, resulting in more adsorption of not only chlorides but also other ions. Thus, the silanol site density of C–S–H strongly influences the transport of ionic species through pores. This may occur in the case of mineral and/or chemical admixture usage in cement, and admixtures to cement change both the amount of C–S–H and the amounts and types of active surface sites. Differences in the diffusivity of chloride in Portland cement paste and slag cement

paste may be due to dissimilar surface site densities of C–S–H. However, details of the surface site densities of C–S–H and the dependence on C/S have not been established. More research is needed on this topic for a detailed understanding the surface chemistry of C–S–H.

3.4 Validation of the model

The validity of the proposed model was established by comparing simulated results from the model with EPMA data measured in this study as well as published data. The simulations used for a cylindrical saturated HCP sample 50 mm in diameter and 30 mm high immersed in one litre of seawater for 91 days. Other details of the simulation are described in section 3.2. Fig. 12 shows the total content of chloride, which includes the chloride content in the pore solution, chemically bound chlorides, and physically adsorbed of chlorides, predicted by the integrated model together with the values measured by EPMA. There is good agreement between the measured and predicted total contents of chloride. The simulation also gives the kinds of chloride (free, physical, and chemical) in the paste, indicated by the broken lines in Fig. 12. Different mechanisms have a significant influence on the total chloride content inside the pores; however, the physical adsorption of chloride controls the total content of chloride in the sample. Further, there is a small peak both in the total content of chloride and in the physically adsorbed chloride near the exposed surface. This can be explained by changes in the concentration of calcium in the pore solution due to dissolution of cement hydrates. The proposed model considers dissolution of cement hydrates via thermodynamic phase equilibrium reactions, and Fig.13 shows the results of the simulated distribution of cement hydrates due to multi–ionic transport into the HCP sample. There is no decalcification of C–S–H, but a high rate of dissolution of portlandite can be noticed near the sample surface that was exposed to chloride solution. The dissolution of portlandite results in a high concentration of calcium in the pore solution near the

surface exposed to chloride, and the calcium concentration decreases with distance from the surface. The changes in calcium concentration lead to changes in adsorption of chloride through the reaction in Eq. (14). Further, excess amounts of both calcium and sulphate ions in the pore solution near the exposed surface relates to the formation of secondary ettringite. The EPMA observations of the element distribution in HCP are shown in Fig. 14. There is high degree of dissolution of elements near the exposed surface. The calcium profile indicates the dissolution of portlandite from the surface towards the inside of the sample as a result of ionic transport. The rise in sulphate concentration near the surface gives experimental evidence for the formation of secondary ettringite. The experimental data for element profiles of sodium and potassium by EPMA mapping exhibit result patterns similar to the simulations (shown in Fig.6). It can be seen that the sodium concentration decreases and the potassium concentration increases when moving away from the exposed surface. Precipitation of Friedel's salt occurs due to dissolution of ettringite and monosulfoaluminate in the presence of chloride, and the region where Friedel's salt forms correlates with the disappearance of monosulfoaluminate. Sulphate ions released from monosulfoaluminate to the pore solution are adsorbed on the surface of C–S–H. Fig. 14 shows that there is no alteration of the cement hydrates at greater distances from the external surface. In addition, the total amount of aluminium does not show large changes inside the HCP. Overall, these results are consistent with the records of other researchers [6–7, 41].

To provide further validation to the proposed integrated model, the model was tested against published EPMA data. Experimental results published by Jensen enable an evaluation of the validity of the proposed model [42]. However, other experimental data were obtained in this study for a more complete documentation. Jensen analyzed chloride ingress into both cement paste and mortar by EPMA [42]. In the simulation discussed here, a saturated HCP was exposed to a 3 % of sodium chloride solution which approximates the sodium chloride concentration in seawater. Thus, upstream concentrations are 3 % NaCl and downstream concentrations are the pore solution concentrations of the

HCP (Table 3). Equilibrated exposure solution (solution for the exposure after attaining equilibrium with C–S–H, portlandite, ettringite, and monosulfoaluminate) enter the pore of the HCP, with the pore size distribution of HCP given in Table 4, and it is further assumed that the shape of the pores is cylindrical. The simulated chloride profile shows good agreement with the EPMA data, as shown in Fig. 15. Jensen modelled the chloride ingress by combining Fick's law with the Freundlich type chloride binding equation [42]. In the Jensen model, the calculated chloride diffusion coefficient for the profile given in Fig. 15 is 22 $*10^{-12}$ m^2/s. In this study, the diffusion coefficient of chloride was determined by measuring the changes in the chloride concentration in the downstream solution with time until a steady state was achieved (described in ref. [13]), and the calculated value for HCP is $7.33*10^{-12}$ m^2/s. There is a large discrepancy between these calculated values of chloride diffusion coefficients and the value in free water (Table 1). However, these calculated values of diffusion coefficients are based on Fick's law without any adjustments to the law. For example, the electric field caused by other ions is not considered. Further, these values are time–dependent diffusion coefficients. Considering the above altogether, it can be expected that these calculated diffusion coefficient values do not accurately predict very long–term chloride ingress into cementitious materials. However, the integrated model presented in this research overcomes this. For very accurate predictions however, additional mechanisms should also be incorporated in the proposed model, and further modifications are needed for a full understanding of the situation in blended cementitious materials.

4. Conclusions

The EDL properties of hydrated cement have a significant effect on adsorption as well as on the transport of aggressive substances through the gel pores, which occupies around thirty percent of the

total volume. An integrated thermodynamic model employing the surface complexation model, the phase–equilibrium model, and the multi–component diffusion model has been proposed to simulate the ionic ingress into hydrated cement paste. Thermodynamic equilibrium between cement hydrates (C–S–H, portlandite, ettringite, and monosulfoaluminate) and contact aqueous solutions is taken into account in the phase–equilibrium model. The interaction of not only chloride but also other ions with C–S–H is considered via the surface complexation model. The equilibrium constant values for physical adsorption of both anions and cations are derived by fitting adsorption and zeta potential data to the model results. The simulated results from the integrated thermodynamic model show that the physical adsorption ions on cement hydrate surfaces, the size of pores, and the surface site density of C–S–H significantly influence the rate of penetration of ionic species through cementitious materials. Furthermore, Fick's second law may not be adequate to predict the amount of penetrating ions into cementitious materials, but it needs a proper formalism that would include multi–species action, phase–equilibrium reaction, and surface complexation reaction. The concentration profile of chloride has been predicted and compared with a measured EPMA profile in this study as well as other published data. A good correlation between measured total content of chloride and simulated values was observed in hydrated cement paste. Furthermore, the model can predict the total chloride as well as other types of chloride. Some future experimental work is considered on the distribution of cement hydrates during multi–ionic transport in order to provide further validation to the proposed model.

Acknowledgement

Authors thank the Japan Society for the Promotion of Science, Grants–in–Aid for JSPS fellows (Research No: 2100930609, Representative: Dr. T. Sato), for funding a part of this present research

work.

References

1. Rui Miguel Ferreira, Probability based durability analysis of concrete structures in marine environments, PhD thesis, University of Minho, School of Engineering, Department of Civil Engineering, 2004.
2. C. Andrade and J. Kropp (Eds.), Testing and Modelling Chloride Ingress into Concrete, Proceedings of the 3rd International RILEM Workshop, Madrid, 2002.
3. C. L. Page, N. R. Short, A. El. Tarras, Diffusion of chloride ions in hardened cement pastes, Cement and Concrete Research 11, 395–406, 1981.
4. E. Samson, J. Marchand, J. –L. Robert, and J. –P. Bournazel, Modelling ion diffusion mechanisms in porous media, International Journal for Numerical Methods in Engineering 46, 2043–2060, 1999.
5. E. Samson *et al.*, Modelling ion and fluid transport in unsaturated cement systems in isothermal conditions, Cement and Concrete Research 35, 141–153, 2005.
6. B. Johannesson, K. Yamada, L–O. Nilsson, Y. Hosokawa, Multi–species ionic diffusion in concrete with account to interaction between ions in the pore solution and the cement hydrates, Materials and Structures 40, 651–665, 2007.
7. Hosokawa *et al.*, A Development of a multi–species mass transport model considering thermodynamic phase equilibrium, International RILEM symposium on concrete modelling: CONMOD'08, Delft, The Netherlands, 2008.
8. F. P. Glasser, J. Marchand, E. Samson, Durability of concrete–degradation phenomena involving detrimental chemical reactions, Cement and Concrete Research 38, 226–246, 2008.

9. S. Goto *et al.*, Cement Science and Concrete Technology, JCA, 36: 49 – 52, 1982.
10. N. Kimura *et al.*, Membrane potential across anion－exchange membranes in acidic solution system. Journal of Colloid and Interface Science 286: 288–293, 2005.
11. J. Z. Zhang, N. R. Buenfeld, Membrane potential and its influence on chloride transport in cementitious materials. In Andrade C, Kropp J. (eds) Testing and modeling the chloride ingress into concrete. 2nd International RILEM workshop. Cedex: RILEM publications S.A.R.L, 33 – 49, 2000.
12. J. Z. Zhang, J. Y. Li, N. R. Buenfeld, Measurement and modelling of membrane potentials across OPC mortar specimens between 0.5 M NaCl and simulated pore solutions, Cement and Concrete Composites 24, 451 – 455, 2002.
13. Y. Elakneswaran, T. Nawa, K. Kurumisawa, Influence of surface charge on ingress of chloride ion in hardened paste, Materials and Structures 42, 83－93, 2009.
14. Y. Elakneswaran, Electrochemical study on the ingress of chloride ion into cement paste, Master thesis, Division of Solid Waste Resources and Geoenviromental Engineering, Graduate School of Engineering, Hokkaido University, JAPAN, 2006.
15. E. Nagele, The zeta–potential of cement, Cement and Concrete Research 15, 453–462, 1985.
16. S. Chatterji and M. Kawamura, Electrical double layer, ion transport, and reactions in hardened cement paste, Cement and Concrete Research 22, 774–782, 1992.
17. L. Nachbaur, P. C. Nkinamubanzi, A. Nonat and J.C Mutin, Electrokinetic properties which control the coagulation of silicate cement suspensions during early age hydration. Journal of Colloid and Interface Science 202, 261–268, 1998.
18. H. Viallis *et al*.: Interation between salts (NaCl,CsCl) and calcium silicate hydrates (C–S–H), J. Phys. Chem. B 103, 5212–5219, 1999.
19. H. Viallis－Terrisse, A. Nonat, J.C. Petit. Zeta–potential study of calcium silicate hydrates interacting with alkaline cations, Journal of Colloid and Interface Science 244, 58–65, 2001.

20. I. Pointeau, P. Reiller, N. Mace, C. Landesman and N. Coreau, Measurement and modelling of the surface potential evaluation of hydrated cement pastes as a function of degradation. Journal of Colloid and Interface Science 300, 33–44, 2006.
21. M. Castellote *et al.*, Oxygen and chloride diffusion in cement pastes as a validation of chloride diffusion coefficient obtained by steady－state migration tests, Cement and Concrete Research 31, 621–625, 2001.
22. S. Goto, D. M. Roy, Diffusion of ions through hardened cement pastes, Cement and Concrete Research 11, 751–757, 1981.
23. S. W. Yu, C. L. Page, Diffusion in cementitious materials: 1. Comparative study of chloride and oxygen diffusion in hydrated cement pastes, Cement and Concrete Research 21, 581–588, 1991.
24. H. Friedmann, O. Amiri, A. Ait – Mokhtar, Physical modelling of the electrical double layer effects on multispecies ions transport in cement–based materials, Cement and Concrete Research 38, 1394–1400, 2008.
25. Y. Elakneswaran, T. Nawa, and K. Kurumisawa, Electrokinetic potential of hydrated cement in relation to adsorption of chlorides, Cement and Concrete Research 39, 340–344, 2009.
26. Ph. Blanc, X. Bourbon, A. Lassin, E.C. Gaucher, Chemical model for cement–based materials: Temperature dependence of thermodynamic function for nanocrystalline and crystalline C–S–H phases, Cement and Concrete Research 40, 851–1468, 2010.
27. C. A. J. Appelo and D. Postma, Geochemistry, groundwater and pollution, CRC Press Taylor & Francis Group, 2009.
28. C. Zhu and G. Anderson, Environmental applications of geochemical modelling, Cambridge University press, 2002.
29. T. Matschei, B. Lothenbach, F. P. Glasser, Thermodynamic properties of Portland cement hydrates in the system $CaO–Al_2O_3–SiO_2–CaSO_4–CaCO_3–H_2O$, Cement and Concrete Research 37, 1379–1410,

2007.

30. D. L. Parkhurst and C. A. J. Appelo, User's guide to PHREEQC (Version 2)— A computer program for speciation, batch－reaction, one－dimensional transport and inverse geochemical calculations, Water－Resources Investigations Report 99–4259, U.S. Geological Survey, 1999.
31. David A. Dzombak and Francois M. M. Morel, Surface complexation modelling: Hydrous Ferric oxide, A Wiley–Interscience Publication, 1990.
32. I. G. Richardson, The calcium silicate hydrates, Cement and Concrete Research 38, 137–158, 2008.
33. T. G. Heath, D. J. Ilett and C. J. Tweed, Thermodynamic modelling of the sorption of radioelements onto cementitious materials, 443–449.
34. C. Anthony, J. Appelo, and Paul Wersin, Multicomponent diffusion modelling in clay systems with application to the diffusion of tritium, iodide, and sodium in opalinus clay, Environ. Sci. Technol 41, 5002–5007, 2007.
35. F. P. Glasser, Role of chemical binding in diffusion and mass transport, in: R. Doug Hooton *et al*. (Eds.), Proceeding Material Science of Concrete. International conference on ion and mass transport in cement－based materials, Toronto, 129–154, 1999.
36. S. Y. Hong and F. P. Glasser, Alkali binding of cement pastes Part I. The C–S–H phase, Cement and Concrete Research 29, 1893–1903, 1999.
37. S. J. Stuart and B. J. Berne, Effects of polarizability on the hydration of the chloride ion, J. Phys. Chem. 100, 11934–11943, 1996.
38. S. J. Stuart and B. J. Berne, Surface curvature effects in the aqueous ionic salvation of the chloride ion, J. Phys. Chem. A 103, 10300–10307, 1999.
39. R. Mills and V. M. M. Lobo, Self–diffusion in electrolyte solutions: a critical examination of data compiled from the literature, Elsevier Science Publishers B. V, 1989.
40. L. Cui and J. H. Cahyadi, Permeability and pore structure of OPC paste, Cement and Concrete

Research 31, 277–282, 2001.

41. Juan Manuel Galindez, Jorge Molinero, On the relevance of electrochemical diffusion for the modeling of degradation of cementititous materials, Cement & Concrete Composites 32, 351–359, 2010.
42. Jensen O. M, Chloride ingress in cement paste and mortar measured by electron probe micro analysis, Technical Report Series R No. 51, Department of Structural Engineering and Materials, The Technical University of Denmark, December 1998.

CAPTIONS

Tables

Table 1 Composition of artificial seawater and self–diffusion coefficients of ions in free water at 20 °C

Table 2 Thermodynamic properties of major cement hydrates at 25 °C used in PHREEQC calculations [26, 29]

Table 3 Measured ionic concentrations in the pore solution of hydrated cement paste

Table 4 Measured pore size distribution of hydrated cement paste

Figures

Fig. 1 Measured ζ and calculated surface potential of C–S–H as a function of pH in calcium hydroxide solution

Fig. 2 Measured ζ of HCP suspensions in chloride solutions

Fig. 3 Measured [36] and predicted adsorption of sodium on C–S–H for C/S ratio of 1.5 as function of sodium concentration

Fig. 4 Change of log_k with C/S ratio of C–S–H for adsorption of sodium or potassium

Fig. 5 Ionic distribution near a charged surface. The surface is in contact with 0.1 M NaCl

Fig. 6 Simulated ionic concentration in the free solution of pores (centre of pore) considering ionic adsorption

Fig. 7 Main cement hydrates distribution during multi–ionic transport in HCP

Fig. 8 Simulated results for dependence of physical adsorption on chloride transport

Fig. 9 Simulated results for dependence of physical adsorption on cation transport

Fig. 10 Simulated results for dependence of pore size on total content of chloride

Fig. 11 Simulated results for dependence of surface site density on total content of chloride

Fig. 12 Comparison between experimental and simulated chloride profiles for HCP after 91 days of seawater exposure

Fig. 13 Simulated main cement hydrates distribution in HCP after 91 days of seawater exposure

Fig. 14 Element profiles determined by EPMA for HCP after 91 days of seawater exposure

Fig. 15 Comparison between experimental [42] and simulated chloride profiles for HCP after 30 days of chloride exposure

Tables

Table 1 Composition of artificial seawater and self–diffusion coefficients of ions in free water at 20 °C

Ion	Concentration (mM)	Diffusion coefficient * 10^{-9} (m^2/s)
Na^+	485	1.16
Cl^-	566	1.81
K^+	10.6	1.75
Ca^{2+}	10.7	0.70
Mg^{2+}	55.1	0.61
SO_4^{2-}	29.3	0.96
pH	8.2	

Table 2 Thermodynamic properties of major cement hydrates at 25 °C used in PHREEQC calculations [26, 29]

Phases	Formula	log_K_T	$\Delta_r H^o$ (kJ/mol)
C – S – H (C/S=1.6)	$Ca_{1.6}SiO_{3.6}$:2.58H_2O + 3.2H^+ → 1.6Ca^{2+} + 2.18H_2O + H_4SiO_4	28.00	–133.31
Portlandite	$Ca(OH)_2$ + 2H^+ → Ca^{2+} + 2H_2O	22.81	–130.11
Ettringite	$Ca_6Al_2(SO_4)3(OH)_{12}$:26H_2O + 12H^+ → 2Al^{3+} + 6Ca^{2+} + 38H_2O + 3SO_4^{2-}	57.73	–389.36
Monosulfoaluminate	$Ca_4Al_2(SO_4)(OH)_{12}$:6H_2O + 12H^+ → 2Al^{3+} + 4Ca^{2+} + SO_4^{2-} + 18H_2O	73.68	–553.08
Friedel'Salt	$Ca_4Al_2Cl_2O_6$:10H_2O + 12H^+ → 2Al^{3+} + 4Ca^{2+} + 2Cl^- + 16H_2O	74.93	–486.20

Table 3 Measured ionic concentrations in the pore solution of hydrated cement paste

Sample	Concentrations, mM					Ionic strength, mM	Debye Length, nm
	Na^+	K^+	Ca^{2+}	Cl^-	SO_4^{2-}		
HCP－0.5,28,0	88.9	74.8	4.8	1.4	0.2	178.3	0.72

Table 4 Measured pore size distribution of hydrated cement paste

		Pore volume, cm^3/g (%)					
		By Nitrogen adsorption	By MIP, cm^3/g (%)				
	Total	1.4– 6 nm	6–10 nm	10–50 nm	50–100 nm	100–1000 nm	>1000 nm
HCP	0.1460	0.012 (8.2)	0.0324 (22.2)	0.0709 (48.6)	0.0198 (13.6)	0.0035 (2.4)	0.0074 (5.1)

Figures

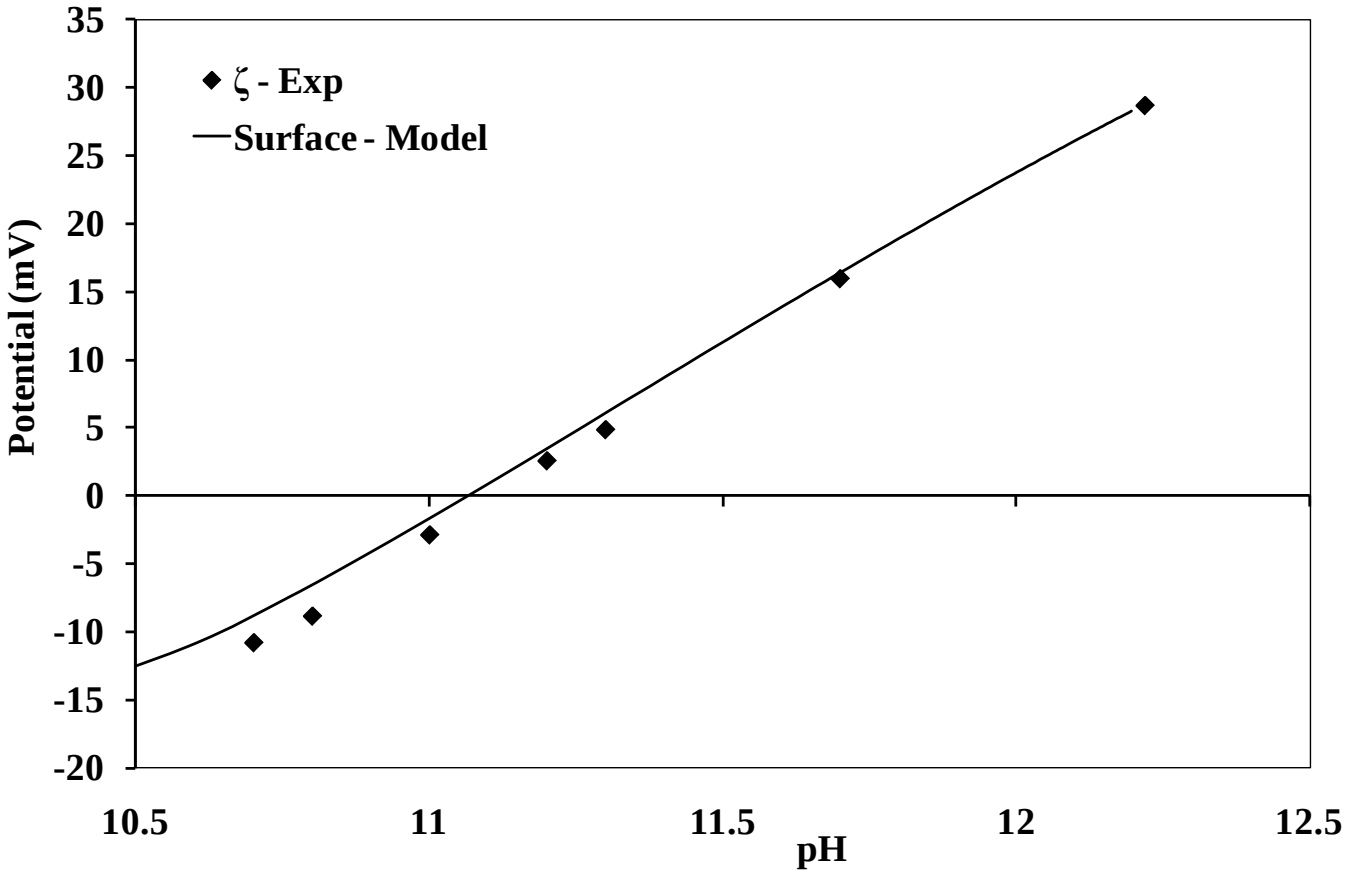

Fig. 1 Measured ζ and calculated surface potential of C–S–H as a function of pH in calcium hydroxide solution

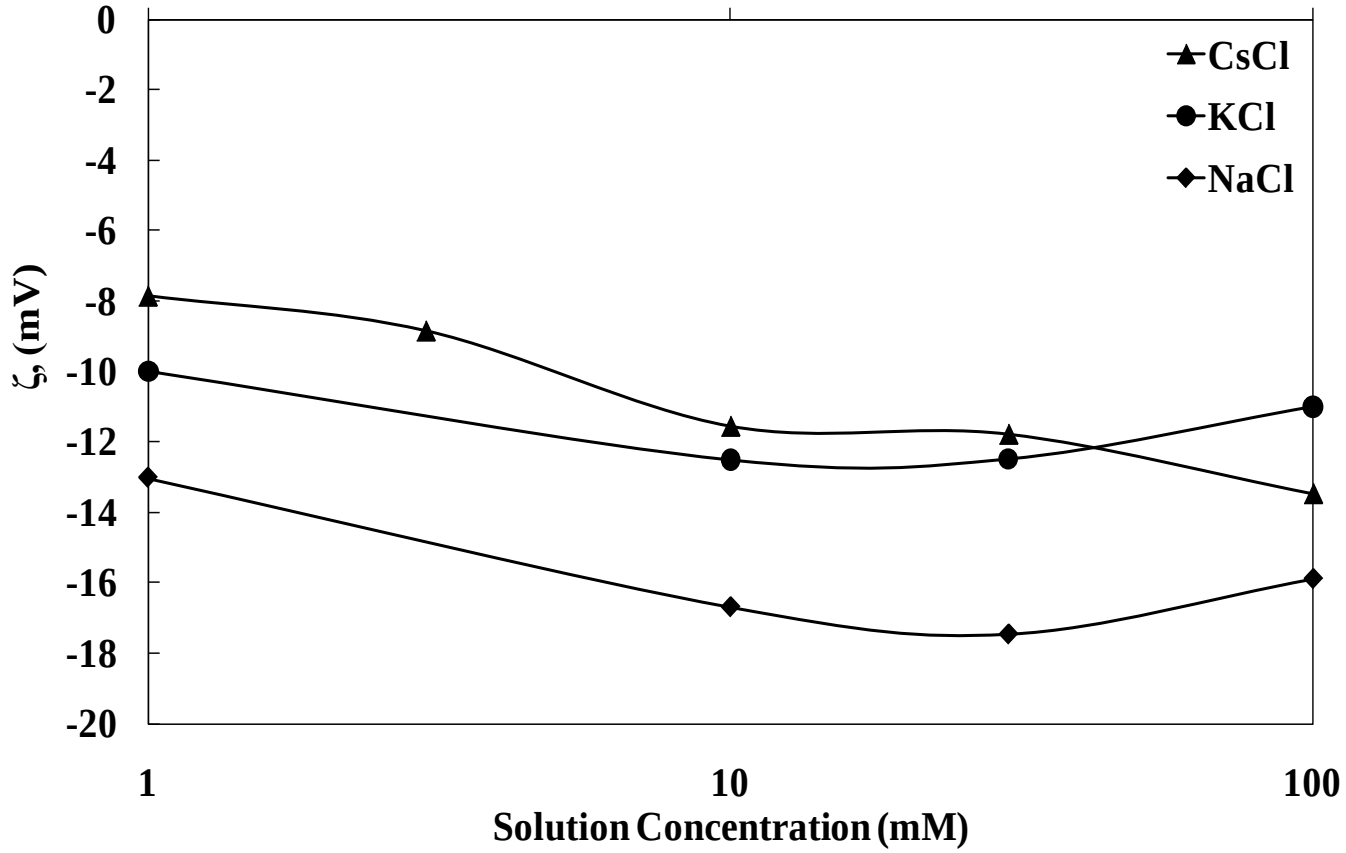

Fig. 2 Measured ζ of HCP suspensions in chloride solutions

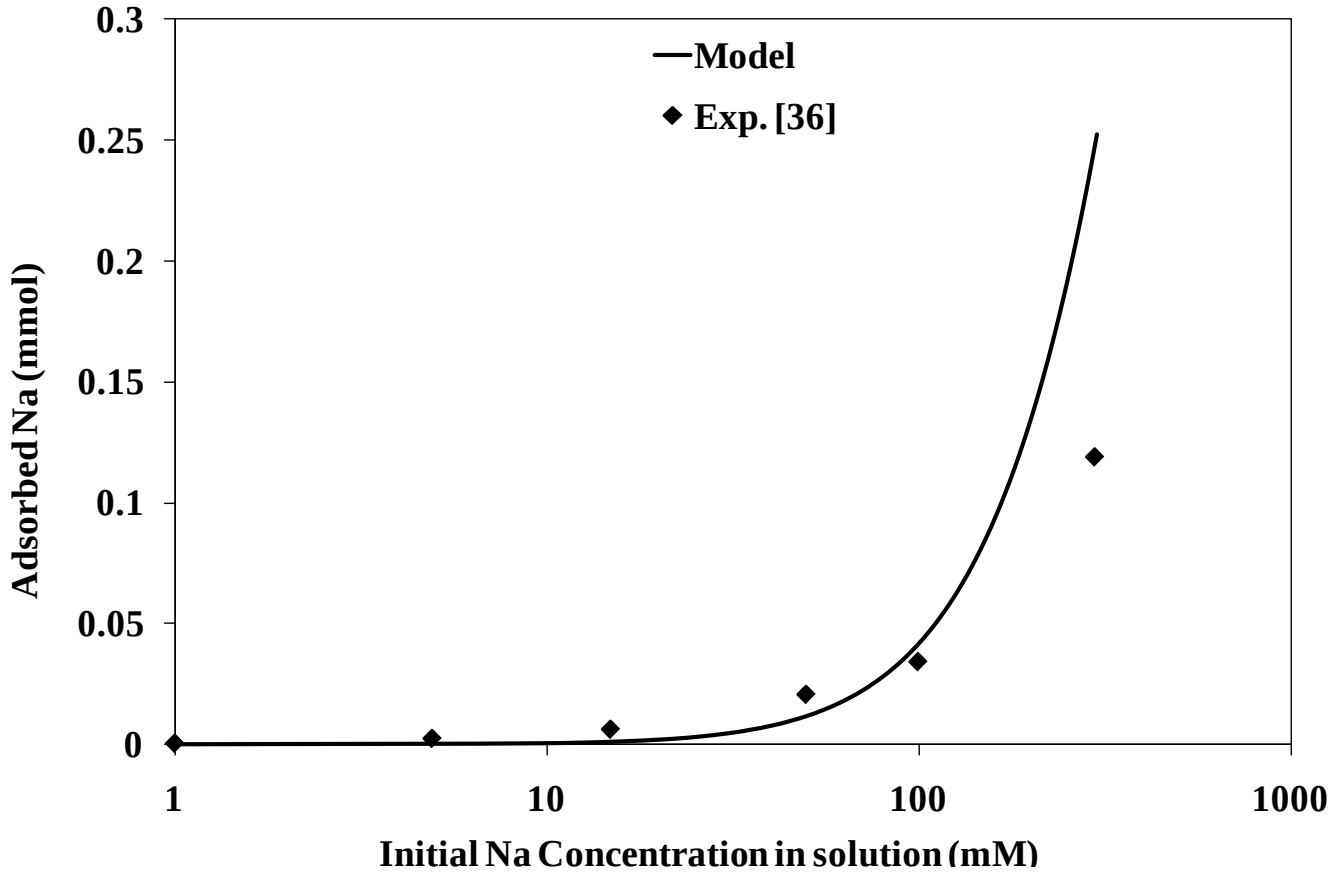

Fig. 3 Measured [36] and predicted adsorption of sodium on C–S–H for C/S ratio of 1.5 as function of sodium concentration

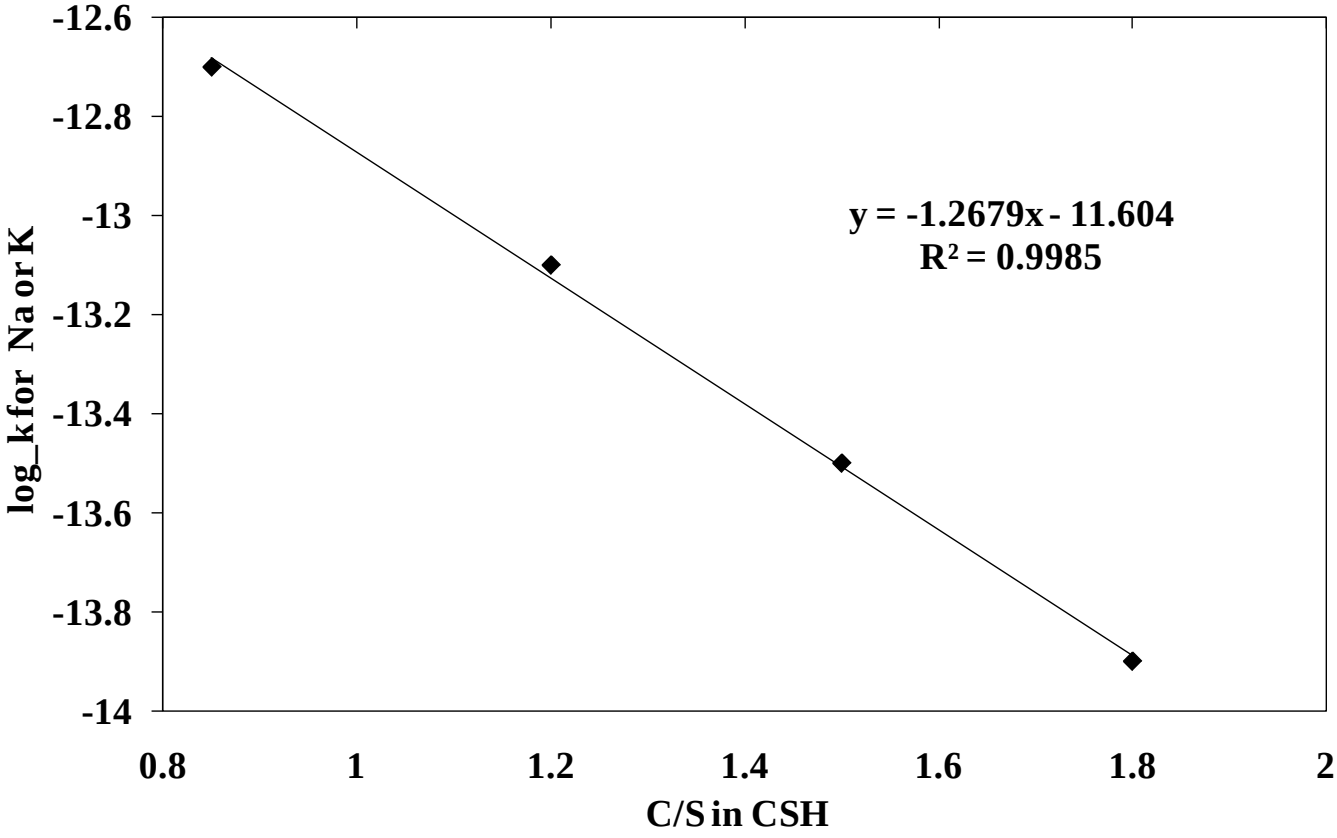

Fig. 4 Change of log_k with C/S ratio of C–S–H for adsorption of sodium or potassium

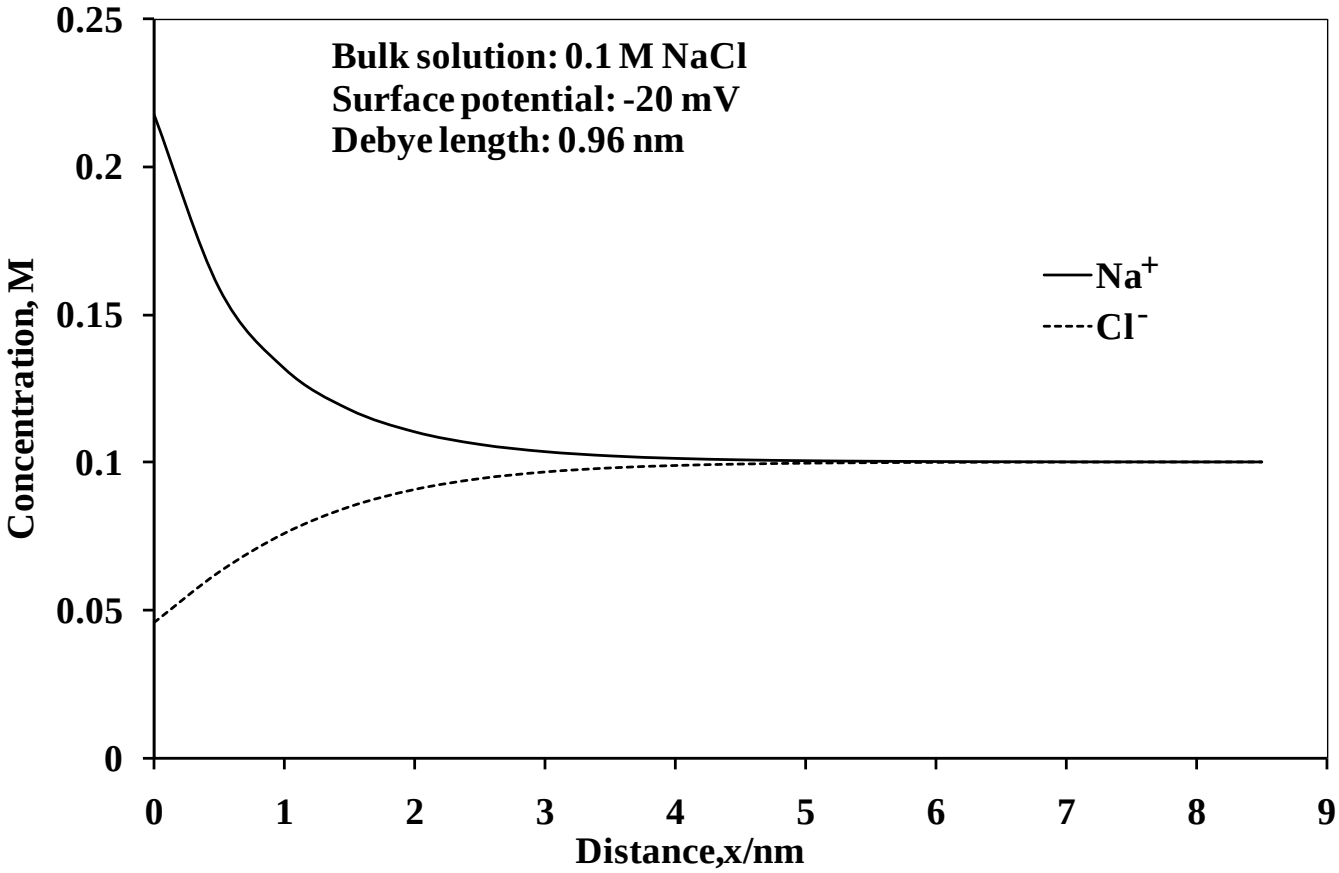

Fig. 5 Ionic distribution near a charged surface. The surface is in contact with 0.1 M NaCl

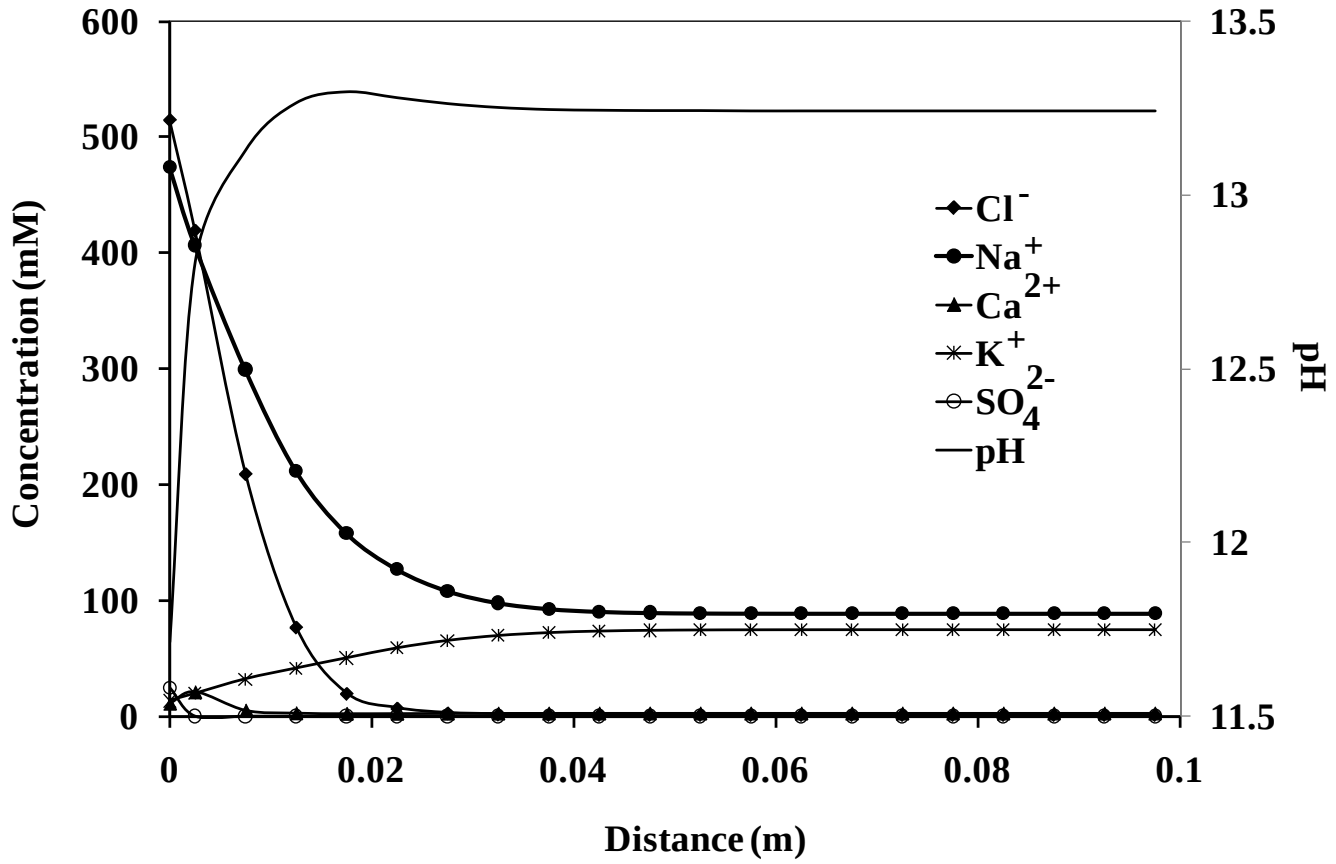

Fig. 6 Simulated ionic concentration in the free solution of pores (centre of pore) considering ionic adsorption

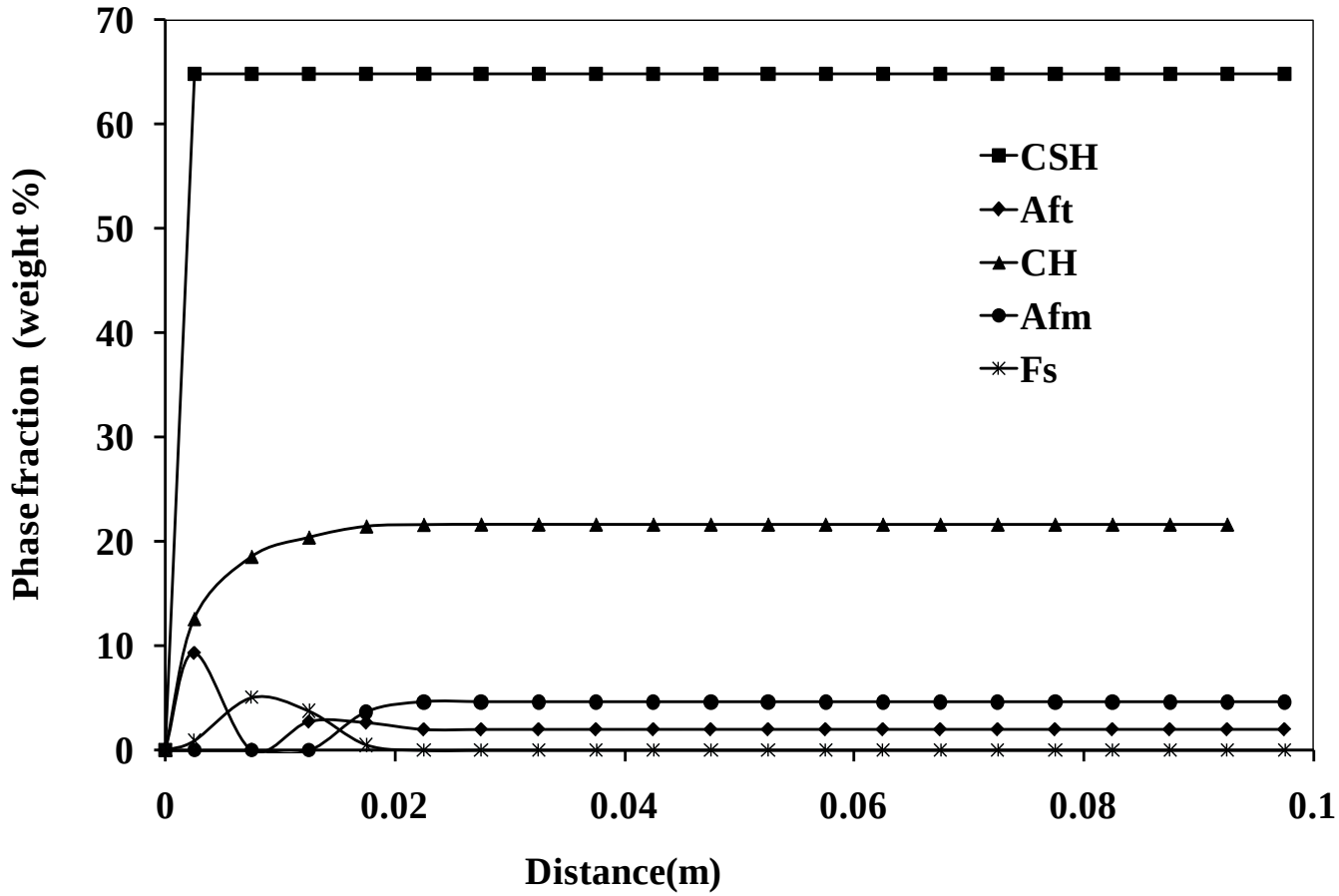

Fig. 7 Main cement hydrates distribution during multi–ionic transport in HCP

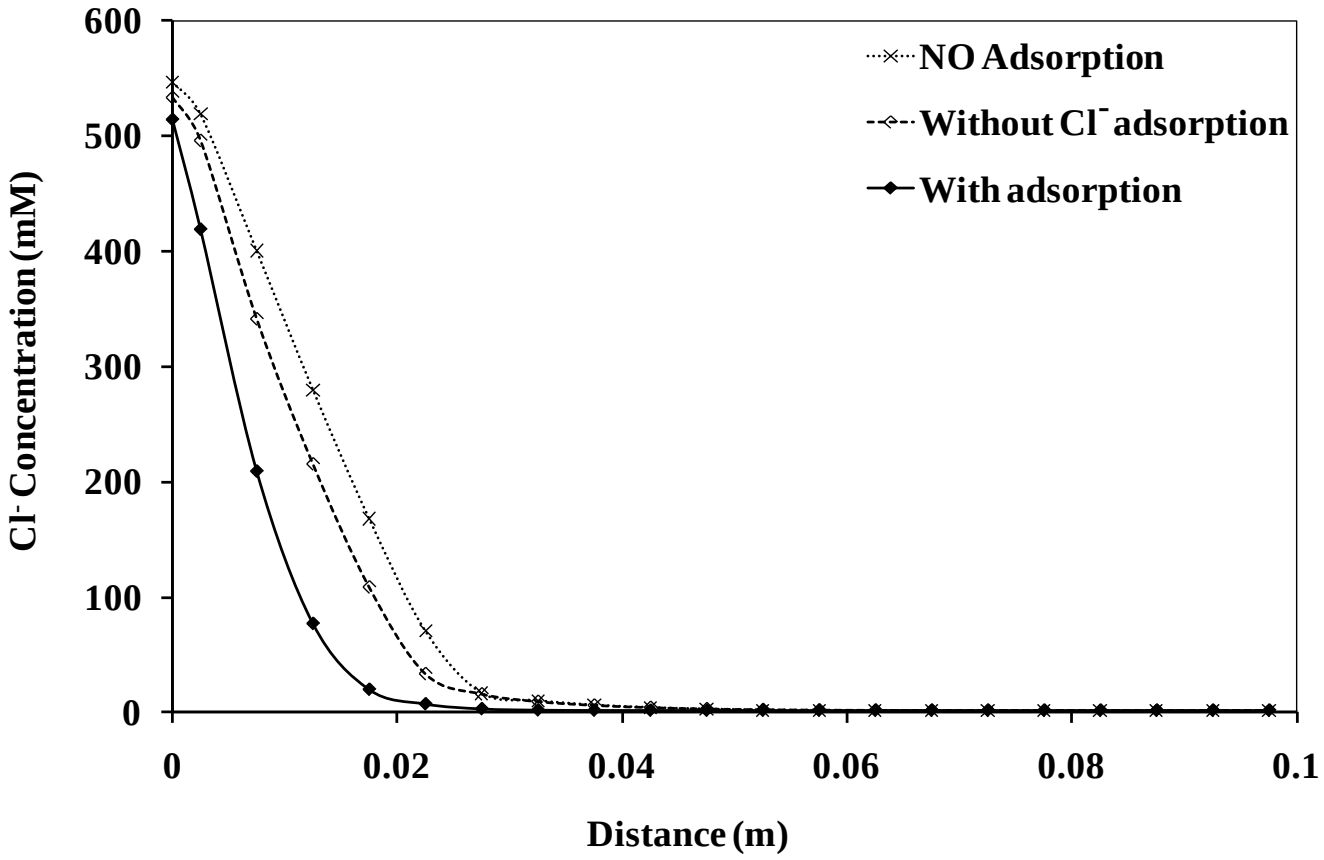

Fig. 8 Simulated results for dependence of physical adsorption on chloride transport

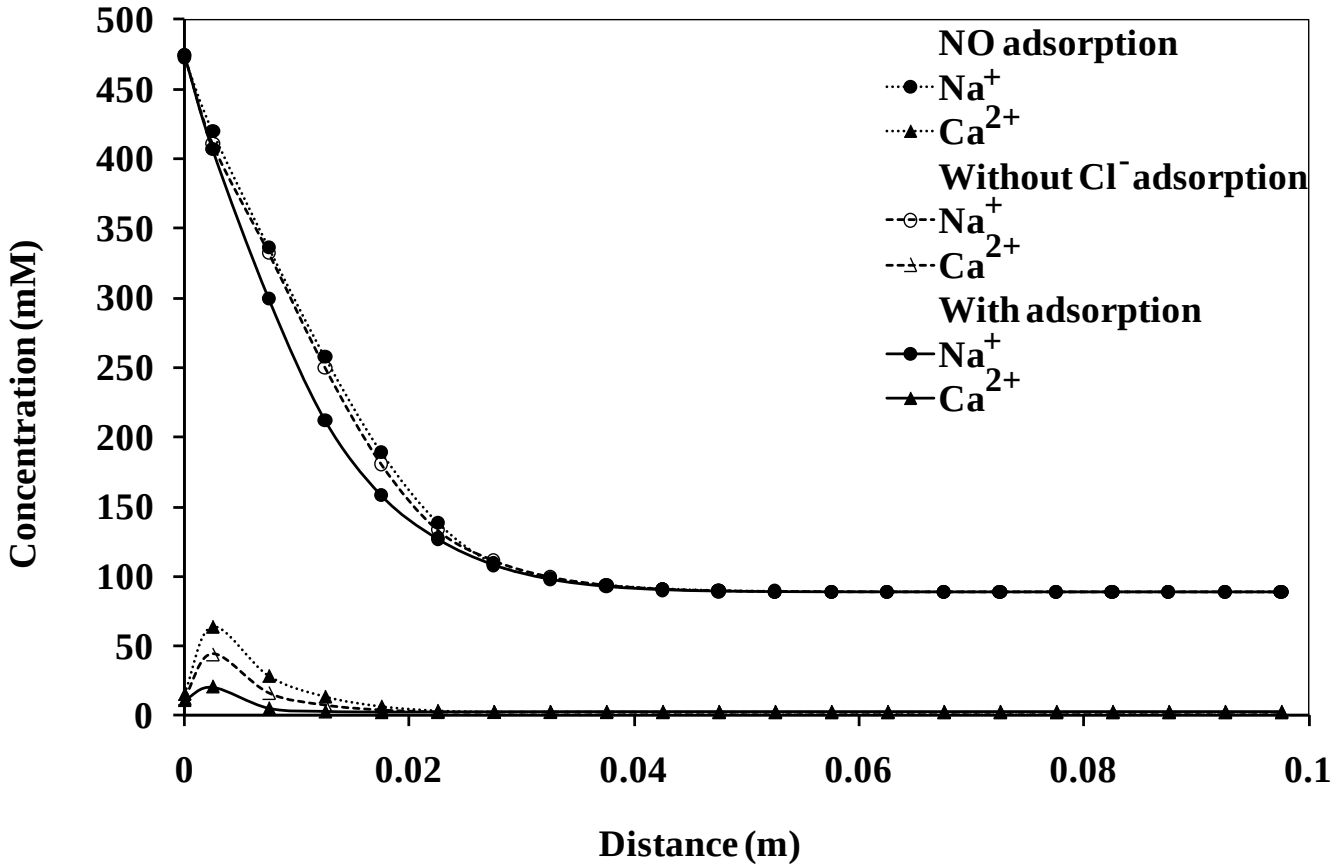

Fig. 9 Simulated results for dependence of physical adsorption on cation transport

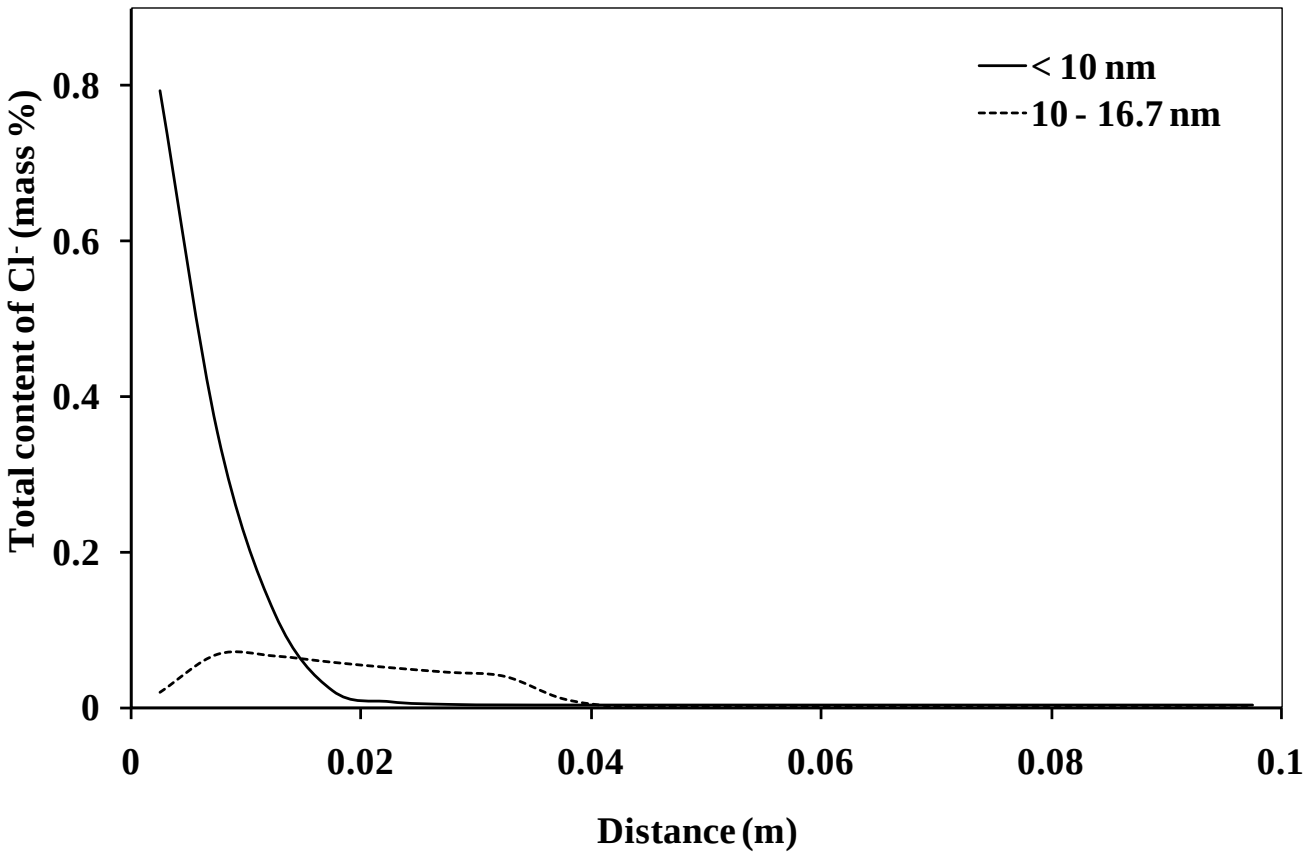

Fig. 10 Simulated results for dependence of pore size on total content of chloride

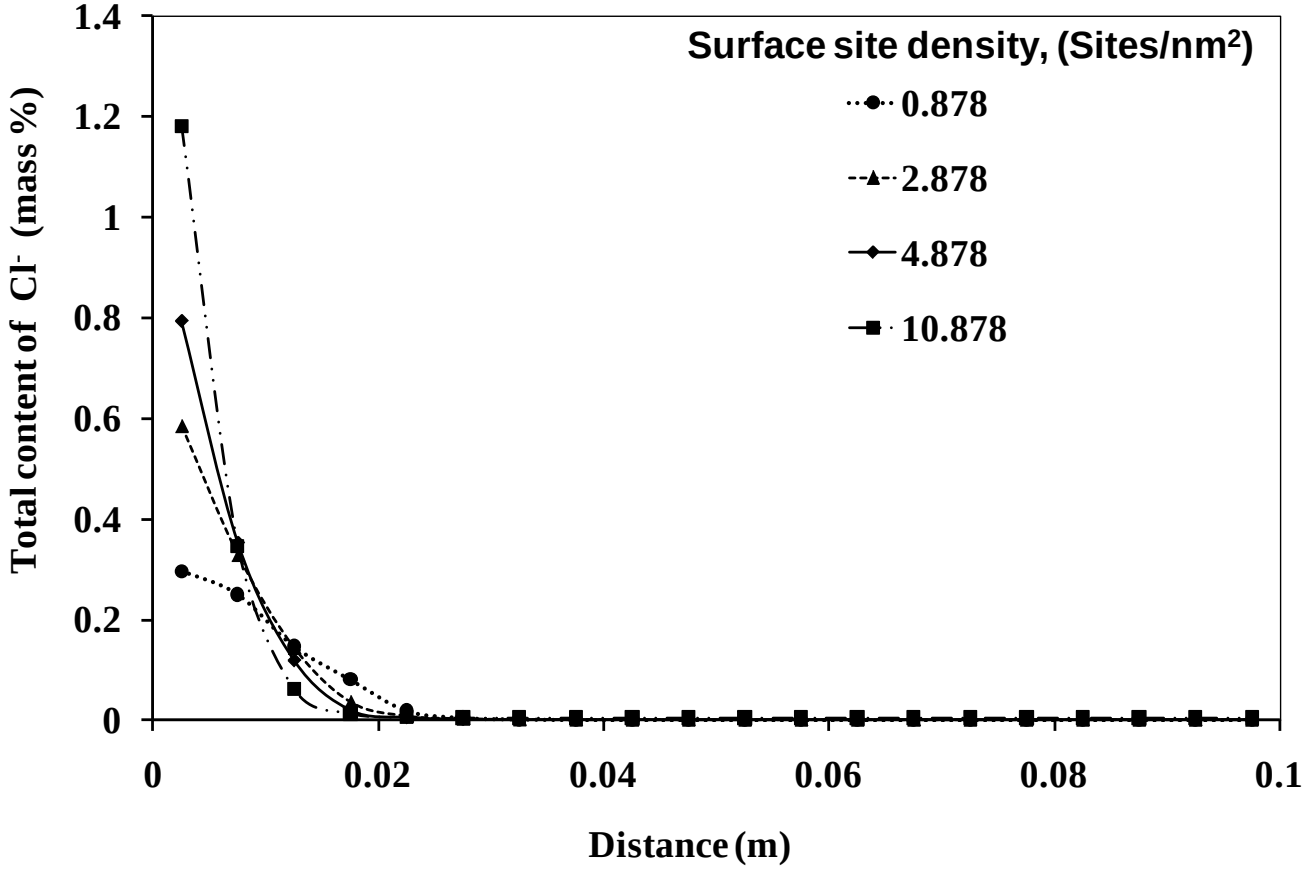

Fig. 11 Simulated results for dependence of surface site density on total content of chloride

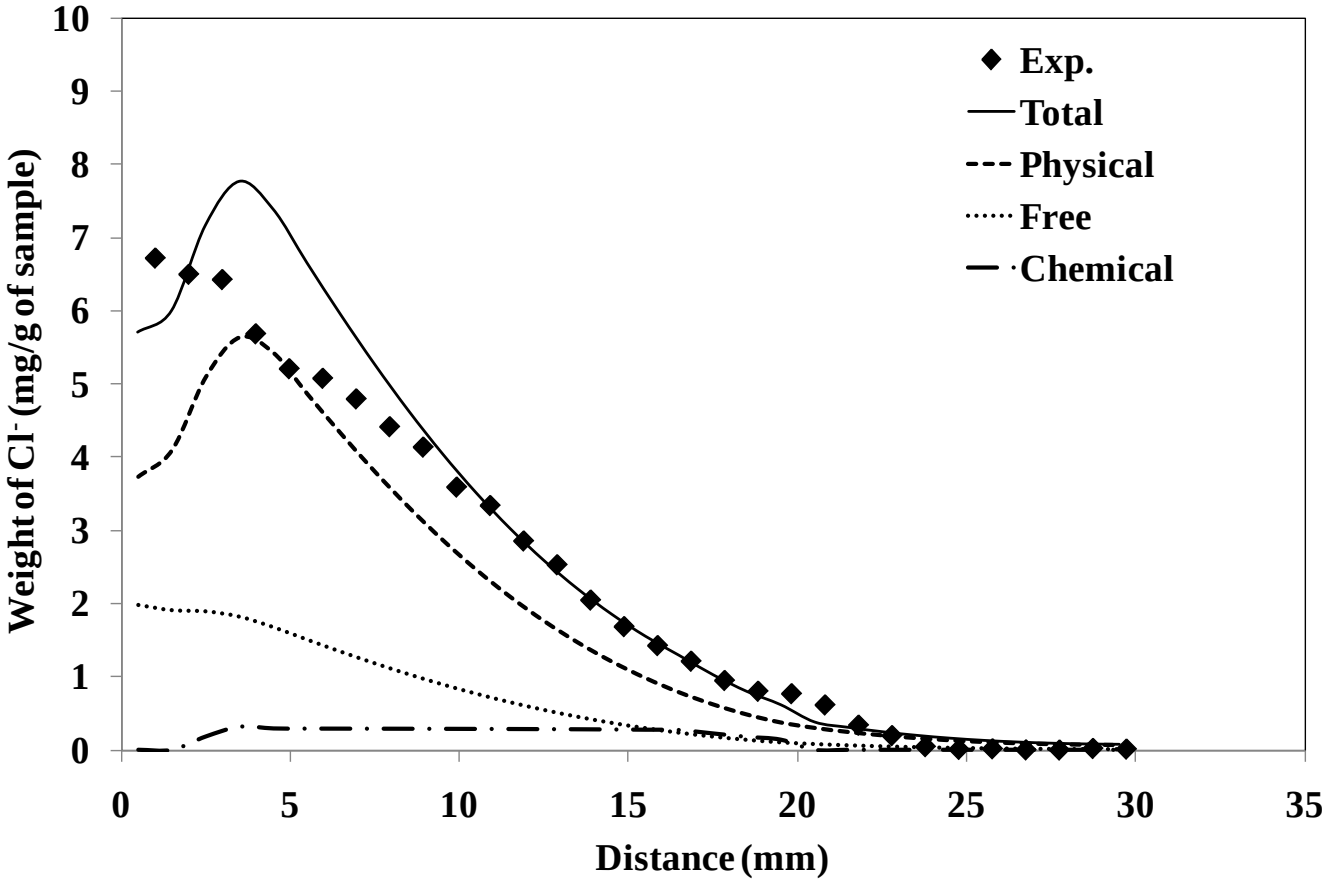

Fig. 12 Comparison between experimental and simulated chloride profiles for HCP after 91 days of seawater exposure

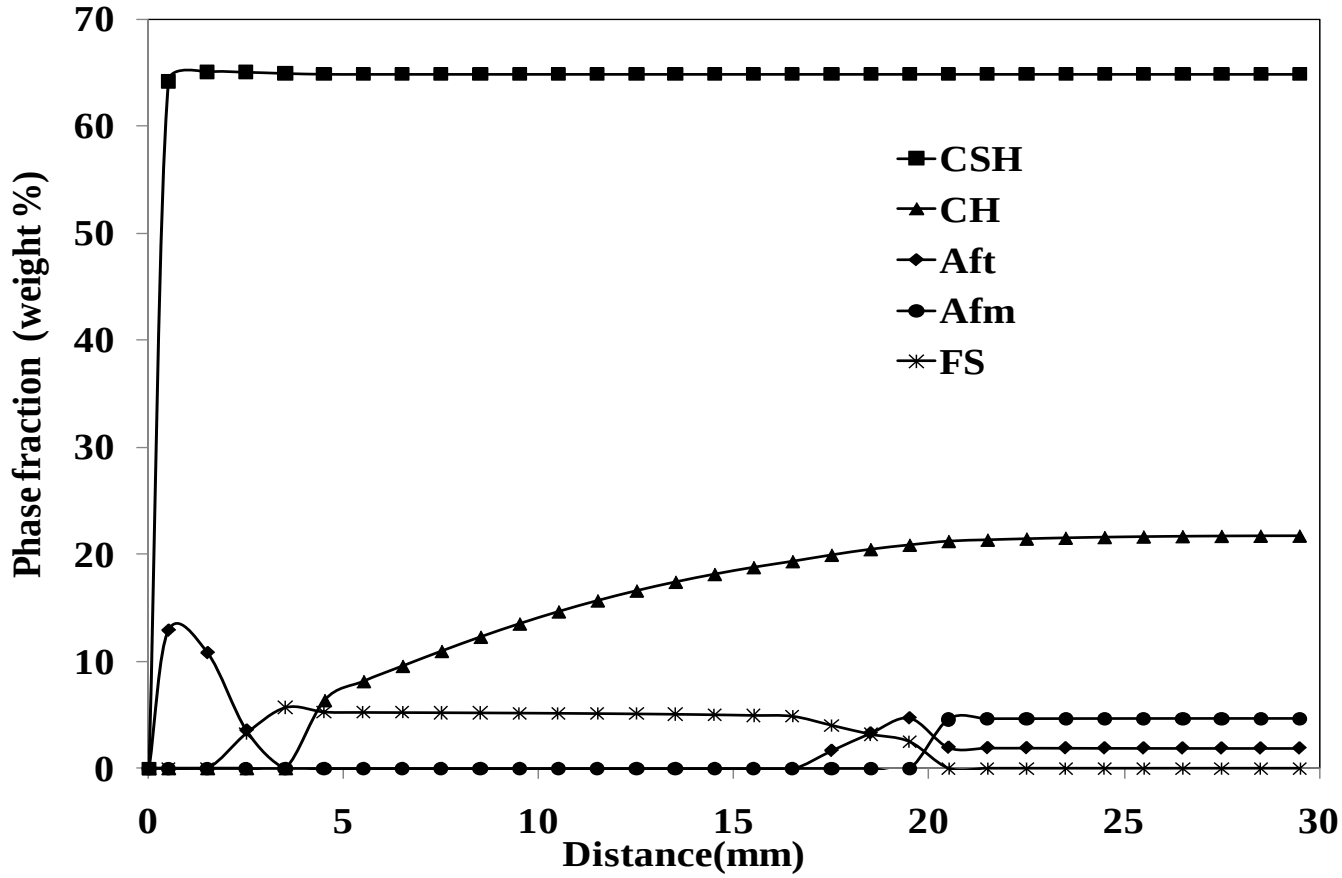

Fig. 13 Simulated main cement hydrates distribution in HCP after 91 days of seawater exposure

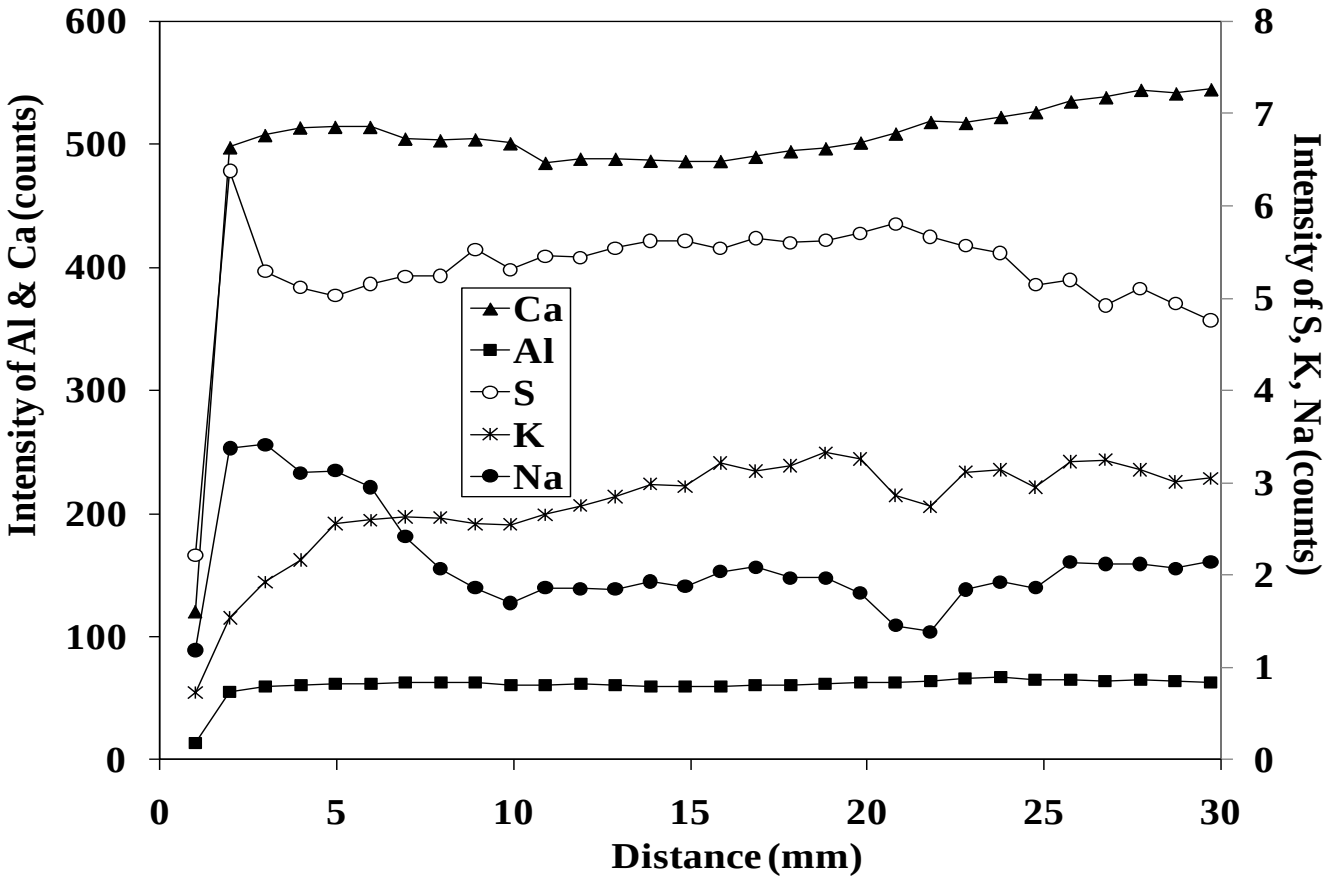

Fig. 14 Element profiles determined by EPMA for HCP after 91 days of seawater exposure

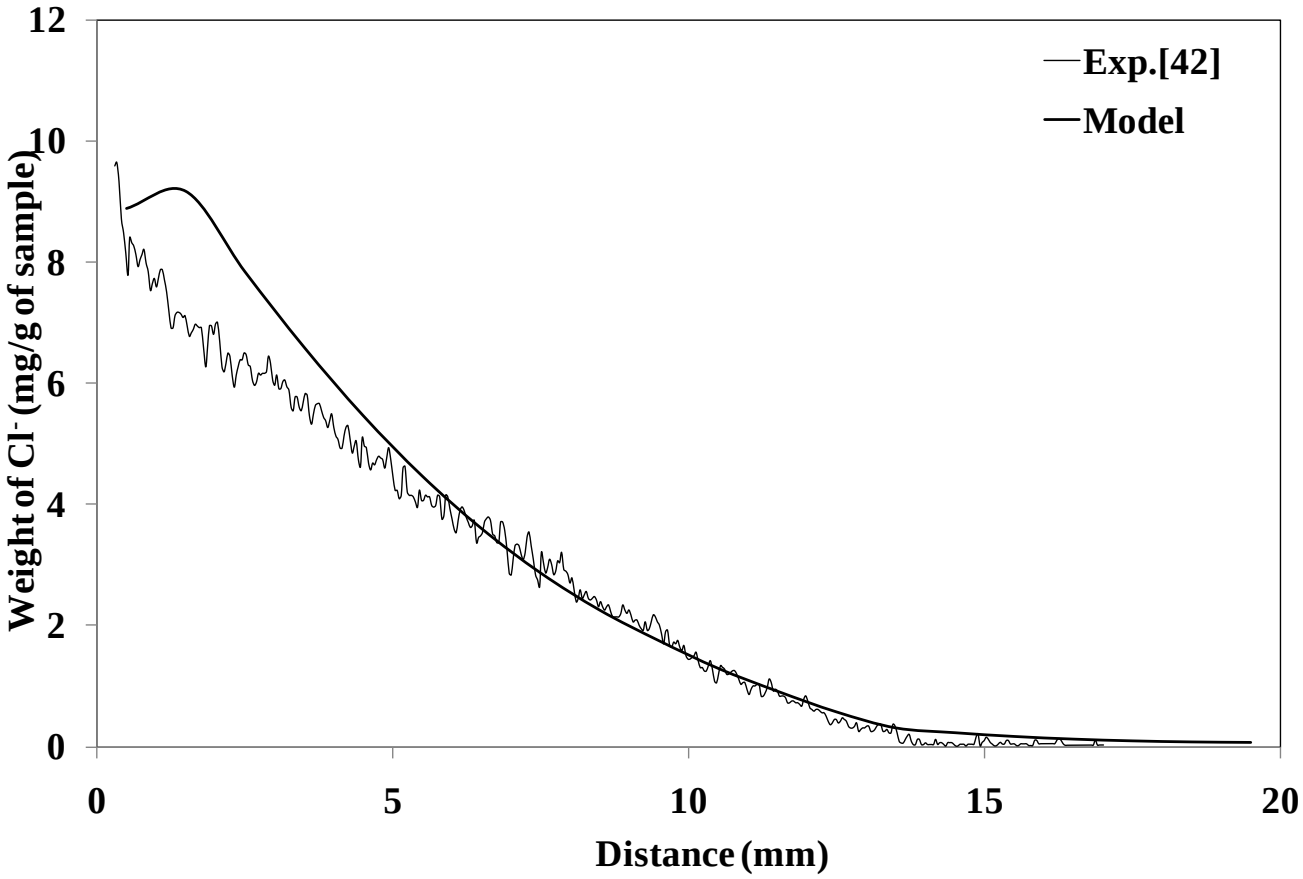

Fig. 15 Comparison between experimental [42] and simulated chloride profiles for HCP after 30 days of chloride exposure